

Plasma Sci. Technol. **20** (2018) 094004 (26pp) https://doi.org/10.1088/2058-6272/aab4f0

Kinetic theory of geodesic acoustic modes in toroidal plasmas: a brief review

Zhiyong QIU[1,4], **Liu CHEN**[1,2] **and Fulvio ZONCA**[1,3]

[1] Institute for Fusion Theory and Simulation and Department of Physics, Zhejiang University, Hangzhou 310027, People's Republic of China
[2] Department of Physics and Astronomy, University of California, Irvine CA 92697-4575, United States of America
[3] ENEA, Fusion and Nuclear Safety Department, C. R. Frascati, Via E. Fermi 45, I-00044 Frascati (Roma), Italy

E-mail: zqiu@zju.edu.cn

Received 5 January 2018, revised 28 February 2018
Accepted for publication 2 March 2018
Published 6 July 2018

Abstract

Geodesic acoustic modes (GAM) are oscillating zonal structures unique to toroidal plasmas, and have been extensively studied in the past decades due to their potential capabilities of regulating microscopic turbulences and associated anomalous transport. This article reviews linear and nonlinear theories of GAM; with emphases on kinetic treatment, system nonuniformity and realistic magnetic geometry, in order to reflect the realistic experimental conditions. Specifically, in the linear physics, the resonant wave–particle interactions are discussed, with the application to resonant excitation by energetic particles (EPs). The theory of EP-induced GAM (EGAM) is applied to realistic devices for the interpretation of experimental observations, and global effects due to coupling to GAM continuum are also discussed. Meanwhile, in the nonlinear physics, the spontaneous GAM excitation by microscale turbulences is reviewed, including the effects of various system nonuniformities. A unified theoretical framework of GAM/EGAM is then constructed based on our present understandings. The first-principle-based GAM/EGAM theories reviewed here, thus, provide the tools needed for the understanding and interpretation of experimental/numerical results.

Keywords: geodesic acoustic mode, kinetic theory, nonlinear physics, energetic particle physics

(Some figures may appear in colour only in the online journal)

1. Introduction

The peculiar role of toroidally and poloidally symmetric zonal structures (ZS) [1–5] and their influence on the overall plasma performance has been well accepted and extensively studied in the past two decades. ZS can regulate microscale drift wave turbulence (DW) [6], including drift Alfvén waves (DAWs), via scattering into short radial wavelength stable domain, and thereby, suppress the DW induced anomalous transport. ZS can, thus, be viewed as the generator of nonlinear equilibria with suppressed turbulence [7, 8], and possibly an important factor in the H-mode confinement [9, 10].

Geodesic acoustic modes (GAM) [11, 12], as the finite frequency counterpart of zonal flow, have been observed in various machines by different diagnostics [13–22] in the search of zero frequency zonal flow (ZFZF) [2], with the linear features such as mode frequency, three dimension mode structure, density perturbation and radial propagation identified. An inverse relation of turbulence level and GAM intensity were often observed, suggesting the GAMs are excited nonlinearly by ambient turbulence, as shown by bicoherence analysis [23–25]. Theoretically, the regulation of DW by ZFZF and/or GAM, is achieved via the spontaneous excitation of ZFZF/GAM by DWs modulational instability [12, 26]. Thus, the nonlinear drive from DWs in the form of Reynolds stress [27] must be strong enough to overcome the threshold conditions due to frequency mismatch and/or dissipations. The nonlinearly generated ZFZF/GAM, in turn, scatter DWs into stable short wavelength domain. Noting the fact that both ZFZF and GAM can be excited by and regulate DWs, and that their respective nonlinear coupling cross-sections based on gyrokinetic predictions are comparable

[4] Author to whom any correspondence should be addressed.

[12, 26], understanding the nonlinear dynamics of DWs and, thus, quantitative prediction of the transport level require careful examination of linear drive/dissipations of GAM, and the possible direct power transfer between GAM and ZFZF.

Due to its finite frequency, GAM can resonate with, and be excited by energetic particles (EPs) [28, 29], analogous to the shear Alfvén wave (SAW) continuum mode excitation by EPs [30]. Though EGAM typically has a radial scale much longer than that of GAM driven by DWs, the possible nonlinear interactions between EGAM and DWs [31, 32] were observed numerically, suggesting EGAM as an active control for DWs. The observed oscillations at twice of GAM/EGAM frequency [33], furthermore, suggest the nonlinear self-couplings of GAMs, including generating GAM/EGAM second harmonic and ZFZF, as demonstrated by numerical simulations [34]. The generation of GAM/EGAM second harmonic [34–36], as an additional dissipation mechanism for GAM/EGAM, and generation of ZFZF as a channel for direct power transfer from GAM/EGAM to ZFZF [36, 37], will affect the branching ratio of GAM and ZFZF generation by DWs, and, as a consequence, DWs nonlinear dynamics.

In this paper, the theoretical investigation of GAM is briefly reviewed, with emphasis on first-principle-based kinetic treatment and realistic geometry. Therefore, the present result can be directly applied to explain experimental observations and numerical simulations in the the proper limits. The rest of the paper is organized as follows. In section 2, the linear properties of GAM are presented, with the fluid derivation and the discussions of GAM continuum given in 2.1, and the kinetic treatment given in section 2.2, emphasizing on the physics picture of wave–particle resonances in the short wavelength limit. The EGAM local and global theories are reviewed in section 3, with applications to several specific cases in realistic devices. Speculations are made on EGAM nonlinear saturation and possible particle losses due to EGAM induced pitch angle scattering. The spontaneous excitation of GAM by DWs is reviewd in section 4, taking ion temperature gradient (ITG) DW in the local limit as an example. The local nonlinear theory is then generalized to GAM excitation by short wavelength collisionless trapped electron mode (CTEM) DW and toroidal Alfvén eigenmode (TAE). Further extension to global theory is also given, considering the system nonuniformities. The GAM/EGAM nonlinear self-coupling, as one important factor for the nonlinear DW dynamics, is also reviewed in section 5. In section 6, a unified theoretical framework of GAM/EGAM is proposed, including the main processes discussed in this paper. Conclusions and discussions are given in section 7.

2. Linear theory of GAM

In this section, we present the linear GAM theory. First, in section 2.1, adopting a fluid approach to illustrate fundamental properties of the GAM continuous spectrum. Afterwards, in section 2.2, introducing kinetic description and the properties of GAM at short wavelengths.

2.1. Fluid theory: GAM continuum and mode conversion to kinetic GAM (KGAM)

In section 2.1, the fluid theory of GAM will be presented [11, 38], with the GAM continuum due to plasma nonuniformity [12, 38] briefly reviewed, as a peculiar feature of GAM. The GAM continuum induced linear absorption [12] and the multiple-scale radial structure [38] have important consequences on the linear decay due to both continuum and Landau damping [38–41], resonant excitation by EPs [42–45] and nonlinear interactions with DW/DAWs [46], as we will discuss in the rest of the paper. A thorough and detailed investigation of GAM continuous spectrum, including phase mixing and mode conversion to KGAM, was presented in [38].

We start with the linearized fluid equations,

$$\partial_t \delta n + \nabla \cdot (n_0 \delta \mathbf{v}) = 0, \tag{1}$$

$$m_i n_0 \partial_t \delta \mathbf{v} = -\nabla \delta P + \delta \mathbf{J} \times \mathbf{B}_0 / c, \tag{2}$$

$$\delta P = \Gamma_e T_e \delta n_e + \Gamma_i T_i \delta n_i, \tag{3}$$

$$\delta \mathbf{E} + \delta \mathbf{v} \times \mathbf{B}_0 / c = 0, \tag{4}$$

where equations (1)–(4) are, respectively, linearized continuity equation, momentum equation, equation of state and Ohm's law; δn is the number density, $\delta \mathbf{v}$ is perturbed velocity, Γ is the appropriate ratio of specific heats, T is the temperature; subscripts e, i denote, respectively, electron and ion species. Other notations are standard.

The governing GAM equation is derived from the flux surface averaged quasineutrality condition,

$$\partial_r \overline{\delta J_r} = 0, \tag{5}$$

with $\overline{(\cdots)} \equiv \int_0^{2\pi} (\cdots) \mathrm{d}\theta / 2\pi$ denoting magnetic surface averaging and the perturbed radial current δJ_r obtained from the poloidal component of momentum equation as

$$\delta J_r = (c/B_0)[n_0 m_i \partial_t \delta v_\theta + (1/r)\partial_\theta \delta P]. \tag{6}$$

Note that in equation (5) we have neglected equilibrium nonuniformity scale with respect to GAM wavelength by dropping the Jacobian of the adopted toroidal flux coordinates that we use throughout this work. Equation (6) consists of two terms, corresponding to, respectively, the polarization current due to finite GAM frequency, and the perturbed diamagnetic current associated with the perturbed pressure gradient in poloidal direction. δv_θ is the GAM radial electric field induced poloidal drift velocity ('zonal flow'), and the perturbed pressure δP is obtained from equation of state, with the perturbed density δn given by the plasma compressibility due to toroidicity, noting the GAM radial wavelength is much shorter than equilibrium scale

$$\delta n = -\frac{c n_0 k_G \overline{\delta \phi}_G \sin\theta}{\omega B_0 R_0}. \tag{7}$$

Equation (7) is the well-known 'upper-down anti-symmetric' density perturbation of GAM in the fluid limit [47]. Combining equations (3), (5)–(7), the radial GAM mode equation

can be derived as:

$$\frac{\partial}{\partial r}\left[\frac{c^2}{B_0^2}m_i n_0 \omega\left(1-\frac{\omega_G^2}{\omega^2}\right)\right]\frac{\partial}{\partial r}\overline{\delta\phi}_G = 0, \tag{8}$$

with $\omega_G^2 \equiv (\Gamma_i T_i + \Gamma_e T_e)/(m_i R_0^2)$ being the GAM frequency in the fluid limit. Note that the coefficient of the highest order derivative can vanish, and thus, the equation is singular at r_0 with $\omega_G^2(r_0) = \omega^2$, suggesting the existence of GAM continuum [12], similar to the well-known shear Alfvén resonance [48, 49].

Equation (8) can be solved and yield the following solution,

$$\delta E_G = A_+ \exp(\mathrm{i}\omega_G(r)t) + A_- \exp(-\mathrm{i}\omega_G(r)t) + \frac{S_0 \exp(-\mathrm{i}\omega_0 t)}{\omega_0^2 - \omega_G^2(r)}, \tag{9}$$

in which the homogeneous solutions correspond to the initial perturbations of GAM continuum, with A_+ and A_- determined from initial condition, and the inhomogeneous solution corresponds to an incoming oscillation, due to, e.g., an external antenna [38, 50]. This term also accounts for EGAM driven away from r_0 [42, 44] and/or nonlinear drive by DW/DAWs [51] in the form of '$S_0 \exp(-\mathrm{i}\omega_0 t)$'. Note that the initial perturbation oscillates at the local GAM frequency $\omega_G(r)$, and two nearby points initially with the same phase will develop a phase difference $\omega_G'(r)\Delta r t$ in time, with Δr being the radial distance and $\omega_G' \equiv \partial_r \omega_G$. Consequently, the radial wavenumber $\sim\omega_G'(r)t$ increases with time, and generates singular mode structures asymptoticly, leading to the phase mixing of $\delta\phi_G \propto 1/t$ [48]. On the other hand, the oscillation energy piles up at r_0, with the mode structure proportional to $1/(r - r_0)$ near the resonant point r_0. Finite absorption of the driving mode energy density by the plasma then occurs and is described by the Poynting flux into the narrow singular layer around r_0, with the absorption power give by equation (18) of [38].

The singular mode structure given in equation (9) also indicates the breakdown of the MHD treatment at very short radial scales, and the necessity of kinetic treatment. Inclusion of the finite ion Larmor radius effects (FLR) [38, 49] will remove the singularity and introduce mode conversion of the singular continuum solution at r_0 to outward propagating KGAM at Airy scales, as discussed in the case of EGAM driven by a spatially broad EP beam [44] in section 3.2.3. Interested readers may refer to [38] for a more thorough and detailed discussion of interesting physics associated with GAM continuous spectrum.

2.2. Kinetic dispersion relation, and Landau damping in the short wavelength limit

The real frequency of GAM given by fluid theory is not satisfactory for explaining experimental results, due to uncertainties induced by the closure with the equation of state for a collisionless plasma; although the dependence on parameters are qualitatively correct. Some key physics, e.g., wave–particle resonances, are missing in fluid model, which, however, play important role in the GAM related physics such as collisionless Landau damping and excitation by EPs as discussed in section 3. In this section, we briefly summarize the main steps in deriving the GAM linear dispersion relation adopting the gyrokinetic framework, while interested readers may refer to a systematic derivation with rigorous orderings presented in [39]. The particle responses derived here, will also be applied in later sections for the nonlinear GAM interactions with microscopic turbulences.

The perturbed particle distribution function δf can be expressed as

$$\delta f_s = (e_s/m_s)\partial_E F_0 \delta\phi + \exp[\mathrm{i}(m_s c)/(e_s B^2)\mathbf{k}\times\mathbf{B}\cdot\mathbf{v}]\delta H,$$

and the nonadiabatic particle responses δH, can be derived from the general gyrokinetic equation [52]:

$$(-\mathrm{i}\omega + v_\parallel\partial_l + \mathrm{i}\omega_d)\delta H_k = -\mathrm{i}\frac{e_s}{m_s}QF_0 J_k \delta L_k - \Lambda^{\mathbf{k}}_{\mathbf{k}',\mathbf{k}''} J_{k'}\delta L_{k'}\delta H_{k''}. \tag{10}$$

Here, $\omega_d = (v_\perp^2 + 2v_\parallel^2)/(2\Omega R_0)(k_r \sin\theta + k_\theta\cos\theta)$ is the magnetic drift frequency for a circular cross section large aspect ratio tokamak, l is the length along the equilibrium magnetic field line, $QF_0 \equiv (\omega\partial_E - \omega_*)F_0$, $E = (v_\perp^2 + v_\parallel^2)/2$, ω_* is the diamagnetic drift frequency with $\omega_* F_0 \equiv \mathbf{k}\cdot\mathbf{b}\times\nabla F_0/\Omega$, $J_k \equiv J_0(k_\perp\rho_L)$ with J_0 being the Bessel function of zero-index accounting for FLR effects, $\rho_L \equiv mcv_\perp/(eB)$ is the Larmor radius, $\delta L = \delta\phi - v_\parallel\delta A_\parallel/c$, $\Lambda^{\mathbf{k}}_{\mathbf{k}',\mathbf{k}''} \equiv (c/B_0)\sum_{\mathbf{k}=\mathbf{k}'+\mathbf{k}''}\mathbf{b}\cdot\mathbf{k}''\times\mathbf{k}'$; and other notations are standard. The second term on the right-hand side of equation (10) is the convective nonlinearity, which will be used in section 4 for the nonlinear interactions between GAM and DW/DAW turbulences. This is the general form of the gyrokinetic equation in Fourier space [52], and its simplified versions in various limits are used in different sections of this paper for the specific problems of interest; e.g., electro-static limit for linear theory of GAM/EGAM and their nonlinear interactions with DW turbulence, and electro-magnetic limit for the nonlinear GAM excitation by TAE. Note that in section 5, where self couplings of GAM/EGAM are reviewed, an extended version of equation (10) including parallel nonlinearity is used, which is usually neglected because it is typically higher order in the gyrokinetic expansion parameter, and its effect correspondingly enters on a longer time scale compared with that of the convective nonlinearity [53, 54].

In this section, for GAM with $n = 0$ and predominantly electro-static perturbation, one has $v_\parallel\partial_l = (v_\parallel/qR_0)\partial_\theta$, $\omega_* = 0$, $\delta L_G = \delta\phi_G$, and $\omega_d = \omega_{dr} \equiv k_r(v_\perp^2 + 2v_\parallel^2)\sin\theta/(2\Omega R_0) \equiv \hat{\omega}_{dr}\sin\theta$ accounting for radial magnetic drift associated with geodesic curvature. Equation (10) in the linear limit, reduces to

$$(-\mathrm{i}\omega + \omega_{tr}\partial_\theta + \mathrm{i}\omega_{dr})\delta H_G = \mathrm{i}\omega\frac{e_s}{m_s}\partial_E F_0 J_G \delta\phi_G,$$

and for thermal plasmas with Maxwellian distribution function, $\partial_E F_0 = -(m_s/T_s)F_0$. The GAM equation is derived

from the quasi-neutrality condition

$$\frac{n_0 e^2}{T_i}\left(1+\frac{T_i}{T_e}\right)\delta\phi_k = \sum_{s=e,i}\langle q_s J_k \delta H_s\rangle_k, \tag{11}$$

with $\langle\cdots\rangle$ denoting velocity space integration.

For GAM with typically $\omega\sim v_{ti}/R_0$, electron response to GAM can be derived, noting $|\omega_{tr,e}|\gg|\omega_G|$, and one has

$$\delta H^L_{G,e} = \frac{e}{T_e}F_0\overline{\delta\phi}_G, \tag{12}$$

which cancels the electron adiabatic contribution in the perturbed distribution function, as expected.

Decomposing the GAM scalar potential as

$$\delta\phi_G = \sum_m \delta\phi_{G,m}e^{im\theta},$$

with $\delta\phi_{G,m}$ obtained from equation (15), the perturbed ion response to GAM, can be derived as [55]

$$\delta H_{G,i} = -\frac{e}{m_i}\omega J_G\partial_E F_0\sum_p\sum_m\sum_l \times\frac{i^{(p-l)}J_l(\hat\Lambda_d)J_p(\hat\Lambda_d)e^{i(m+l+p)\theta}\delta\phi_{G,m}}{\omega-(l+m)\omega_{tr}}. \tag{13}$$

Here, we have assumed well circulating ions with constant $v_\parallel$, $|\omega|\gg\omega_{b,i}$ with $\omega_{b,i}\sim\sqrt{\epsilon}\omega_{tr,i}$ being the trapped ion bounce frequency and $\epsilon\equiv r/R_0\ll 1$ the inverse aspect ratio, $\hat\Lambda_d\equiv\hat\omega_{dr}/\omega_{tr}\equiv k_r\hat\rho_d$ with $\hat\rho_d\equiv\hat v_d/\omega_{tr}$ the drift orbit width and $\hat v_d\equiv(v_\perp^2+2v_\parallel^2)/(2\Omega R_0)$, and the $e^{-i\hat\Lambda_d\cos\theta}=\sum_l(-i)^l J_l(\hat\Lambda_d)e^{il\theta}$ expansion is applied to derive equation (13). Note that equation (13) is the general particle response to GAM, and it can be used to obtain EP response in section 3.

Different orderings can be taken for non-resonant and resonant ions to further simplify the general response of equation (13). For non-resonant bulk ions, with $v\sim v_{ti}\equiv\sqrt{2T_i/m_i}$, we have $|\omega_{tr,i}/\omega_G|\sim 1/q\ll 1$ and $|\omega_d/\omega|\sim k_r\rho_{ti}\ll 1$. Here, $\rho_{ti}\equiv m_i c v_{ti}/(eB_0)$. As a result, the mode structure and dispersion relation of GAM determined by non-resonant thermal plasma response can be derived by substituting the ion response, equation (13), into quasi-neutrality condition, and applying the $\omega_{tr}\ll\omega$ and $\hat\Lambda_d\ll 1$ limits. One then derives, the Hermitian part of GAM dispersion function

$$D_R = \left[1-\left(\frac{7}{4}+\tau\right)\frac{v_{ti}^2}{\omega^2R_0^2}+\hat b\frac{v_{ti}^2}{\omega^2R_0^2}\left(\frac{31}{16}+\frac{9}{4}\tau+\tau^2\right) -\frac{v_{ti}^4}{\omega^4R_0^4q^2}\left(\frac{23}{8}+2\tau+\frac{\tau^2}{2}\right) -\hat b\frac{v_{ti}^4}{\omega^4R_0^4}\left(\frac{747}{32}+\frac{481}{32}\tau+\frac{35}{8}\tau^2+\frac{\tau^3}{2}\right)\right]\hat b. \tag{14}$$

With the subscript R denoting real part, $\tau\equiv T_e/T_i$, and $\hat b\equiv k_\perp^2\rho_{ti}^2/2$. Equation (14), is derived based on the $|k_r\rho_L|\ll 1$ and $1/q^2\ll 1$ expansion, which is usually satisfied in the parameter region where GAM related physics are important. The perturbed GAM scalar potential, can then be derived from quasi-neutrality condition as

$$\delta\phi_G = \overline{\delta\phi}_G\left\{1-\left[1-\hat b\left(\frac{3}{2}+\tau\right)\right]\tau\frac{\omega_{dt}}{\omega}\sin\theta -\left[\frac{7}{4}+\tau-\hat b\left(\frac{13}{4}+\frac{19}{4}\tau+2\tau^2\right)\right]\tau\frac{\omega_{dt}^2}{2\omega^2}\cos 2\theta -\left[\frac{9}{4}+\frac{7}{8}\tau-\left(\frac{9}{4}+\frac{7}{4}\tau+\frac{\tau^2}{2}\right)\cos 2\theta\right]\tau\frac{\omega_{dt}^3}{\omega^3}\sin\theta -\left(\frac{\tau^2}{2}+\tau\right)\frac{\omega_{dt}\omega_{tt}^2}{\omega^3}\sin\theta\right\}, \tag{15}$$

with the terms proportional to $\hat b$ accounting for FLR effects, ω_{dt}/ω for FOW effects and ω_{tt}/ω for parallel ion compressibility. Here, $\omega_{dt}\equiv k_r\rho_{ti}v_{ti}/R_0$ and $\omega_{tt}\equiv v_{ti}/(qR_0)$.

The collisionless Laudau damping of the toroidally symmetric GAM, is mainly induced by the thermal ion transit harmonic resonances. Noting the $\omega\gg\omega_{tr,i}\gg\omega_{b,i}$ ordering, the 'number' of transit harmonics involved in the process is related to the ratio of GAM wavelength compared to the ion drift orbit width, as demonstrated by equation (13). The Landau damping of GAM due to primary transit resonance ($|\omega|=|\omega_{tr}|$), was investigated in [56], which was then extended to small but finite drift orbit width regime, with $|\omega|=2|\omega_{tr}|$ resonances taken into account [57]. It was shown by TEMPEST simulations [58, 59] that higher order transit harmonic resonances becomes increasingly more important as one further increases $|k_r\hat\rho_d|$ (e.g., by increasing q at fixed $k_r\rho_L$ [58, 59]). Therefore, it was noted that the 'number' of particles that resonate with $\omega=(l+m)\omega_{tr}$ transit harmonic is proportional to $|J_l(\hat\Lambda_d)J_{l+m}(\hat\Lambda_d)F_0(v_{\parallel,\mathrm{res}})|$ from equation (13) with $v_{\parallel,\mathrm{res}}=qR_0\omega_G/(l+m)$. Deriving the GAM Landau damping rate for short wavelength KGAM, which is preferentially excited via DW interactions, then becomes challenging due to the non-trivial task of summing up all the relevant transit harmonic resonances. An alternative approach was developed in [12], which is equivalent to adding up all the transit harmonic resonances. Detailed derivations and interpretations were given in later publications [39, 45]. The anti-Hermitian part of the GAM dispersion function in the short wavelength limit ($k_r\rho_{ti}q^2\gg 1$) is then given as

$$D_I = \sqrt{2}\left[1-2\hat b+\frac{\omega_{dt}^2}{\omega^2}\left(1+\sqrt{2}\tau\left(\frac{7}{4}+\tau\right)\right) +\frac{\omega\omega_{tt}^2}{24}\left(-\frac{4}{\omega_{dt}^3}+\frac{\omega}{\omega_{dt}^4}\right)\right]\exp\left(-\frac{\omega}{\omega_{dt}}\right). \tag{16}$$

Note that, even though D_I is proportional to $\exp(-\omega/\omega_{dt})$ and the leading order resonant particle response is $\delta H_{\mathrm{res}}\propto 1/(\omega-\omega_d)$, the underlying resonant condition is not a 'drift resonance'. The wave–particle energy exchange is due to the summation of all the transit harmonic resonances, as clarified in great detail in [45]. The real frequency and collisionless damping rate of GAM, can then be derived from equations (14) and (16), with FLR and FOW effects properly accounted for. The present approach to the wave–particle

resonances in the short wavelength limit has broad applications in, e.g., EP anomalous transport by ITG DW [60, 61] and short wavelength EGAM excitation [45].

The GAM dispersion relation can be modified by various effects, such as the connection length affected by equilibrium magnetic geometries including aspect ratio [62, 63] and elongation [62–64], kinetic electrons [65, 66] and $m = 2$ electro-magnetic component due to finite $\beta \equiv 4\pi P_0/B_0^2$ [67–71]. The latter issue is connected with our analysis of the vorticity equation below, i.e., equation (51), where finite electromagnetic component in the field line bending term (first term therein) comes from the curvature coupling term (third term therein), due to the combined effect of geodesic curvature and the up–down anti-symmetric density perturbation. Interested readers may refer to the original publications for details.

3. EP induced GAM: resonant excitation, global mode structure and nonlinear saturation

Due to its finite real frequency, GAM can resonate with EPs and be driven unstable by velocity space anisotropic EPs if the EP resonant drive is strong enough to overcome the dissipations due to, e.g. thermal ion induced Landau damping and/or continuum damping. Since its observation in experiments [28, 29, 72, 73], EGAM has attracted attention due to its potential application as active control of DW turbulences [31, 32, 74, 75]. The theoretical interpretation was first given in [76], taking an EP beam with slowing down distribution in energy and localized Gaussian in pitch angle. The mechanism for EGAM drive, is similar to the well-known beam-plasma instability (BPI) in a strongly magnetized plasma, where a positive energy plasma mode is coupled to a negative energy beam mode [77]. The local EGAM theory was then generalized to different cases depending on EP source drive [45, 78–83]. Worthwhile being mentioned are the sharp gradient in pitch angle induced by prompt loss leading to fast EGAM onset discussed in [77], and a theory considering not fully slowed down EP beam [84] to explain the EGAM experiments in large helical device (LHD) with low collisionality [72].

While the continuous spectrum is one of the key features of GAM [12], the theories mentioned above on EGAM ignored it by focusing on deriving the local dispersion relation [77, 84, 85]. Thus, the associated radial structures, which were expected to play important roles in the EP linear and nonlinear dynamics [4, 38, 86], were neglected. The effect of GAM continuum on EGAM excitation was first pointed out in [42], where, by matching across the singular resonant layer with the GAM continuous spectrum, a model dispersion relation of global EGAM was obtained, demonstrating the finite drive threshold due to the GAM continuum damping and the similarity to EP mode (EPM) [30]. The global properties of EGAM depend on the relative scale lengths of GAM continuum and EP density profile, and thus, on the coupling of EGAM to GAM continuum. The excitation of EGAM by a radially localized EP beam was then investigated in [43]. With the EP beam localized away from the position where the mode frequency matches that of the GAM continuum, the continuum damping is minimized, and the obtained global EGAM radial mode structure shows that EGAM is self-trapped by the localized EP beam [43, 87], with an exponentially small tunneling coupling to propagating KGAM, resulting in an exponentially small EGAM excitation threshold. The case of a radially broad EP beam with a density profile scale length comparable with the characteristic scale length of GAM continuous spectrum was considered in [44], which is more relevant to realistic tokamak conditions, and the excited EGAM is shown to strongly couple to GAM continuum, as expected.

In this section, the major progresses in linear EGAM analytical theory are reviewed, with the local stability properties discussed in section 3.1. The global EGAM theory [43, 44] considering the EP profile and coupling to GAM continuum is presented in section 3.2. Speculations on EGAM nonlinear saturation and EP transport are made in section 3.3.

3.1. Local EGAM theory

In this section, the local EGAM theory will be discussed, with the case of the slowing down distribution in energy and single pitch angle EP investigated in section 3.1.1, elucidating also the similarity of EGAM to the well-known BPI. In section 3.1.2, we will discuss the case with a not fully slowed down EP beam due to NBI in a plasma with low collisionality [72, 84]; while the case with a sharp gradient in pitch angle due to prompt loss of injected neutral beam [77] is discussed in section 3.1.3. These two cases may relate to the fast onset of EGAMs in experiments [77, 84]. In the analysis through out section 3, small but finite T_e/T_i is assumed, such that $\omega_{tr,e} \gg \omega_G$ and GAM/EGAM scalar potential is dominated by $m = 0$ component. Note that, despite the apparent contradiction of this assumption with LHD experimental observations [72] at high electron temperature, the theoretical analysis remains qualitatively unchanged.

The EGAM equation is derived from the surface averaged quasi-neutrality condition

$$-\frac{e}{m_i}n_0 k_r^2 \frac{1}{\Omega_i^2}\left(1 - \frac{\omega_G^2}{\omega^2} - \frac{G}{2}k_r^2\rho_{ti}^2\right)\overline{\delta\phi}_G + \overline{\delta n_h} = 0, \quad (17)$$

with the thermal plasma response obtained in the previous sections, G is due to thermal ion FLR/FOW effect, and its expression is given in [43] (equation (31) therein). The perturbed EP density, $\overline{\delta n_h}$, is defined as

$$\overline{\delta n_h} = 2\pi B_0 \sum_{\sigma=\pm 1}\int \frac{E\mathrm{d}\Lambda\mathrm{d}E}{|v_\parallel|}\overline{\left[\frac{e}{m}\frac{\partial F_{0,h}}{\partial E}\overline{\delta\phi}_G + J_G\delta H_h\right]}, \quad (18)$$

with $\Lambda \equiv \mu/E$ denoting the particle pitch angle, and $\mu \simeq v_\perp^2/(2B_0)$ the magnetic moment. The EP nonadiabatic response, δH_h, is given by the $m = 0$ component of the general solution, equation (13), due to the $T_e/T_i \ll 1$ limit

assumed here

$$\delta H_h = -\frac{e}{m_i}\omega J_G \partial_E F_{0,h} \sum_p \sum_l \times \frac{i^{(p-l)} J_l(\hat{\Lambda}_{d,h}) J_p(\hat{\Lambda}_{d,h}) \mathrm{e}^{\mathrm{i}(l+p)\theta} \overline{\delta\phi}_G}{\omega - l\omega_{tr,h}}. \quad (19)$$

Note that, $k_r \equiv -\mathrm{i}\partial_r$ is the radial derivative operator, so equation (17) can be readily applied to study the global EGAM problem. In the local limit with $\hat{\Lambda}_{d,h} \ll 1$, i.e., the EP drift orbit width is much smaller than the characteristic wavelength of EGAM, the primary transit resonances $\omega = \pm\omega_{tr,h}$ dominate, and thus, the optimal ordering for EGAM excitation is $T_h/T_i \sim q^2$. Keeping only $l = 0, \pm 1$ transit harmonics, and assuming well circulating EPs, one then has

$$\overline{\delta n_h} = A \int \frac{(2 - \Lambda B_0)^2}{\sqrt{1 - \Lambda B_0}} \frac{B_0 \mathrm{d}E \mathrm{d}\Lambda E^{5/2} \partial_E F_{0,h}}{2E(1 - \Lambda B_0) - \omega^2 q^2 R_0^2}. \quad (20)$$

Here, $A = \sqrt{2}\pi c e^2 k_r^2 \overline{\delta\phi}_G / (B_0 \Omega_i)$.

Equation (17), thus, with perturbed EP density given by equation (20) and thermal ion FLR effects neglected is the general equation describing local EGAM excitation by well circulating EPs, with the specific cases characterized by different equilibrium EP distribution function $F_{0,h}$. EGAM excitation by bounce resonance of deeply trapped EPs is investigated in [88], and will not be discussed here due to length constraints.

3.1.1. Excitation by EP with slowing down distribution function. We start with the general case of EP distribution being slowing down in energy and localized in pitch angle [43, 76]. This reflects that EP collisions with thermal electrons (slowing down) are more efficient than that with ions (pitch angle scattering) at high EP velocity, and is consistent with the $\beta_h/\tau_{\mathrm{SD}} \sim \beta_c/\tau_E$ ordering for plasma heated by EPs. Here, τ_{SD} is the typical slowing down time and τ_E is the energy confinement time. This case was first investigated by Fu [76], with the final eigenmode equation (corresponding to equation (17) here) solved numerically to show that the unstable branch is characterized by a frequency lower than the local GAM frequency. Here, in order to make further analytic progress, we take a single pitch-angle slowing-down distribution for the EPs [43]; i.e., $F_{0,h} = c_0(r)\delta(\Lambda - \Lambda_0)H_E$, where $c_0(r) = \sqrt{2(1 - \Lambda_0 B_0)}\, n_b(r) / (4\pi B_0 \ln(E_b/E_c))$, $n_b(r)$ is the density of the EPs beam, E_b and E_c are, respectively, the EP birth and critical energies [89], $\delta(x)$ is the Dirac delta function, and $H_E = \Theta(1 - E/E_b)/(E^{3/2} + E_c^{3/2})$, with $\Theta(1 - E/E_b)$ being the Heaviside step function. Noting that generally $E_b \gg E_c$, the local EGAM dispersion relation can be derived as:

$$\mathscr{E}_{\mathrm{EGAM}} = -1 + \omega_G^2/\omega^2 + N_b[C \ln(1 - \omega_{tr,b}^2/\omega^2) + D(\omega_{tr,b}^2/\omega^2)/(1 - \omega_{tr,b}^2/\omega^2)] = 0; \quad (21)$$

where $\omega_{tr,b} = \sqrt{2E_b(1 - \Lambda_0 B_0)}/(qR_0)$ is the EP transit frequency at birth energy, $N_b \equiv n_b\sqrt{1 - \Lambda_0 B_0}\, q^2/(4\ln(E_b/E_c)n_c) \propto \beta_h$ (noting $T_h/T_i \sim q^2$) $C \equiv (2 - \Lambda_0 B_0)(-2 + 5\Lambda_0 B_0)/(2(1 - \Lambda_0 B_0)5/2)$ $C \equiv (2 - \Lambda_0 B_0)(-2 + 5\Lambda_0 B_0)/(2(1 - \Lambda_0 B_0)5/2)$ and $D = \Lambda_0 B_0(2 - \Lambda_0 B_0)^2/(1 - \Lambda_0 B_0)^{5/2}$.

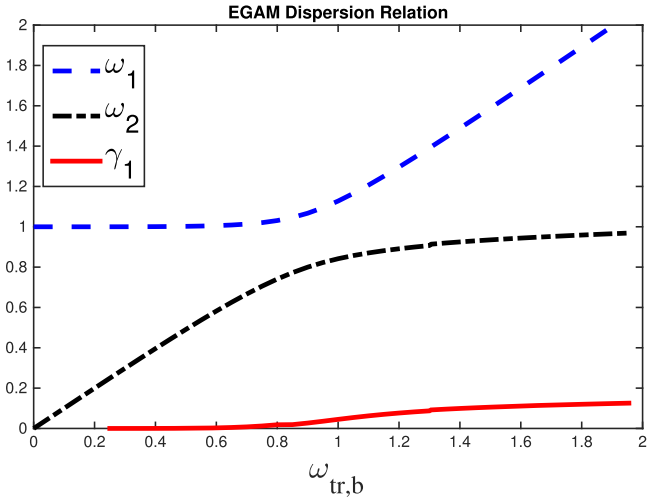

Figure 1. EGAM dispersion relation.

In equation (21), the first term in the EP response (i.e., the logarithmic term) corresponds to resonant EP drive and the second term contributes to frequency shift from local GAM continuum frequency. As a result, the EGAM instability requires $C > 0$, i.e.,

$$\Lambda_0 B_0 > 2/5. \quad (22)$$

Equation (21) can be solved numerically, and the numerical solution is shown in figure 1. The real frequency and growth rate versus $\omega_{tr,b}$ are plotted in units of ω_G. It is shown that, when $\omega_{tr,b}$ is far away from ω_G, there are two branches with frequency determined by GAM and $\omega_{tr,b}$, respectively. As $\omega_{tr,b} \simeq \omega_G$, these two branches are strongly coupled, and reconnect. The solid curve is the linear EGAM growth rate corresponding to the unstable branch ω_2, the dotted–dashed curve. The unstable mode frequency is always lower than the local GAM frequency [76], consistent with experimental observations [29]. The similarity of EGAM to the well-known BPI can be clearly seen from this figure. Note that the similarity of the EGAM in three dimensional tokamak to the BPI in a 1D strongly magnetized plasma is not coincidental. The similarity lies in the fact that, due to the toroidally symmetry mode structure and low frequency, the toroidal angular momentum P_ϕ and mangetic moment μ are conserved, and EGAM is essentially quasi-1D with the dynamics only in (J, θ) space. Here, $J \equiv \int v_\parallel \mathrm{d}l$ is the action conjugate to θ (second adiabatic invariant). This similarity provides insights into, not only the linear physics of EGAM, but also EGAM nonlinear dynamics [38, 79, 90] due to wave–particle phase space nonlinear interactions.

3.1.2. Excitation by not fully slowed down ion beam. The EGAM observed in the LHD [72] during tangential neutral beam injection encountered some difficulties in the comparison with theoretical predictions [43, 76], because the EP birth energy (∼170 keV) is much higher than that

predicted for wave–particle resonance [43], and the observed EGAM frequency can be higher than local GAM frequency. The interpretation was given in [84], noting that EGAM onset time is shorter than the slowing down time ($\tau_{\rm SD} \sim 9$ s) of injected neutral beam due to the peculiar discharge condition with high temperature ($T_e \sim 7$ KeV), low plasma density ($n \sim 0.1 \times 10^{19}\,{\rm m}^{-3}$) [72]. In that work [84], a local theory of EGAM excitation by a not fully slowed down EP beam is investigated. It is shown that the instability drive comes from the positive velocity space gradient in the low-energy end of the EP distribution function [84], in addition to the velocity space anisotropy [76]. For the sake of simplicity, the helicity of the device is ignored and large aspect ratio is assumed, consistent with the experimental observation in the center of the device using heavy ion beam probe [72]. The EP distribution function is given as

$$F_{0,h} = \frac{c_0 H(E_b - E) H(E - E_L)}{E^{3/2} + E_c^{3/2}} \delta(\Lambda - \Lambda_0),$$

which is derived exactly from Fokker–Planck equation with only slowing down collisional operator, and an EP source term with single pitch angle and birth energy. Here, $c_0 = \Gamma_b \tau_{\rm SD}/(4\pi)$ with Γ_b being the NBI particle flux, $E_L \simeq E_b \exp(-2t/\tau_{\rm SD})$ is the time dependent lower energy end of the distribution function, and the modification of the EP distribution function due to interaction with EGAM is ignored.

The dispersion relation can then be derived as

$$\begin{aligned} &-1 + \omega_G^2/\omega^2 + \pi B_0 q^2 c_0/(\sqrt{2} n_0) \\ &\quad \times [C(\ln(1 - \omega_{tr,b}^2/\omega^2) - \ln(1 - \omega_{tr,L}^2/\omega^2)) \\ &\quad + D(1/(1 - \omega_{tr,b}^2/\omega^2) - 1/(1 - \omega_{tr,L}^2/\omega^2))] = 0. \end{aligned} \tag{23}$$

Here, $\omega_{tr,b}$ and $\omega_{tr,L}$ are the transit frequencies defined at E_b and E_L, respectively. Note that, as discussed in the previous section for the slowing down case, the logarithmic singularity at $\omega_{tr,b}$ is destabilizing given $\Lambda_0 B_0 > 2/5$ and thus $C > 0$, and the simple pole at $\omega_{tr,b}$ will only contribute to modulate the EGAM frequency. However, for the not fully slowed down distribution function, considered here, the simple pole at $\omega_{tr,L}$ is also destabilizing and, thus, there is no threshold in pitch angle.

The dispersion relation can be solved numerically as a function of $\tau = t/\tau_{\rm SD}$, and yields the slow temporal evolution of the excited EGAM due to the slowing down of the EP beam. $\omega_{tr,b} = 3\omega_G$ is taken. There are three branches; a GAM branch with $\omega_r \simeq \omega_G$, a lower beam branch with $\omega_r \simeq \omega_{tr,L}(t)$; and an upper beam branch, with $\omega \simeq \omega_{tr,b}$.

The real frequency and growth rate for $\Lambda_0 B_0 < 2/5$ are shown in figures 2 and 3, respectively. We can see that, only the LBB is unstable. In this case, the logarithmic term is stabilizing [43]; thus, the EGAM discussed here is similar to BPI, which, however, has a double pole instead of the simple pole as in the present case. However, when $\omega_{tr,L}$ becomes smaller than ω_G by a finite amount, the growth rate of LBB decreases to zero as the contribution of the simple pole

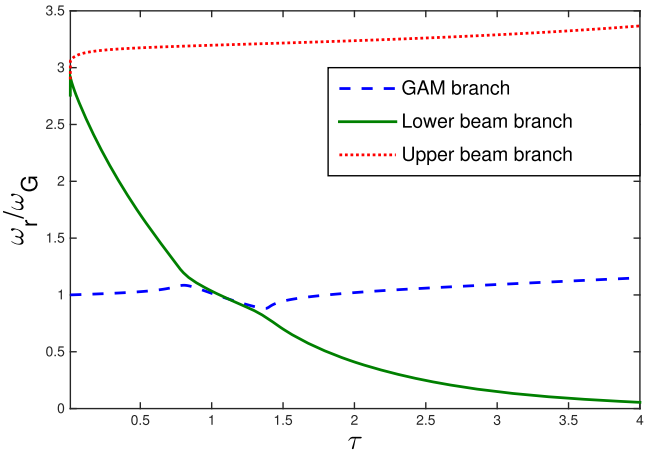

Figure 2. (Reproduced from figure 3 of [84].) Real frequency for $\Lambda_0 B_0 < 2/5$.

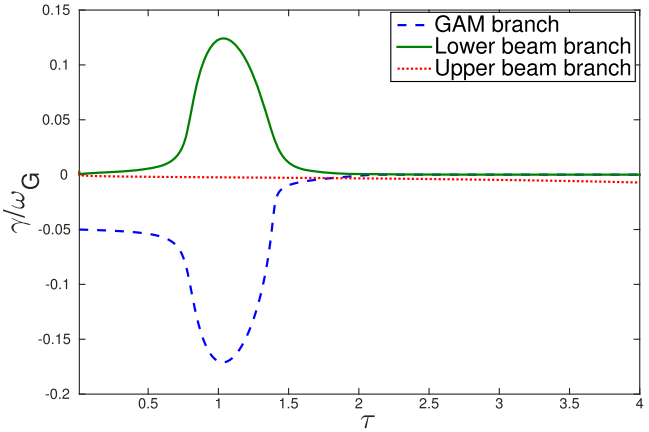

Figure 3. (Reproduced from figure 4 of [84].) Growth rate for $\Lambda_0 B_0 < 2/5$.

becomes vanishingly small, similar to that of BPI. The strong instability at $\omega_L(t) \simeq \omega_G$ may provide an explanation for the fast growth of EGAM observed experimentally. We also note that the frequency of the unstable LBB can be significantly larger than ω_G, as is shown in figure 2. This may explain the higher-frequency branch of EGAM observed in LHD [72].

On the other hand, for $\Lambda_0 B_0 > 2/5$, i.e., $C > 0$, the real frequencies and growth rates are shown, respectively, in figures 4 and 5. The EGAM problem can be understood as a double-beam plasma instability, with the two singularities (logarithmic singularity at $\omega_{tr,b}$ and simple pole at $\omega_{tr,L}$) contributing at different values of $\omega_{tr,L}/\omega_G$. The major difference with the previous case with $\Lambda_0 B_0 < 2/5$ is that, as $\omega_{tr,L}$ further decreases ($\tau > 1.5$), the growth rate decays very slowly, due to the contribution of the destabilizing logarithmic term.

Note that a similar explanation was given in [82], assuming a positive slope in the distribution function due to finite charge exchange time. The interpretation given here, with slight modification to the one discussed in section 3.1.1, can recover all the peculiar features of the LHD EGAM experiment, and the theory can be applicable to potential

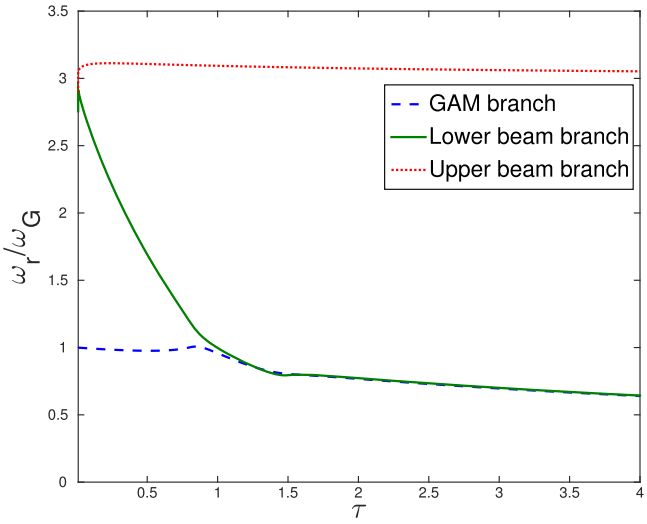

Figure 4. (Reproduced from figure 1 of [84].) Real frequency for $\Lambda_0 B_0 > 2/5$.

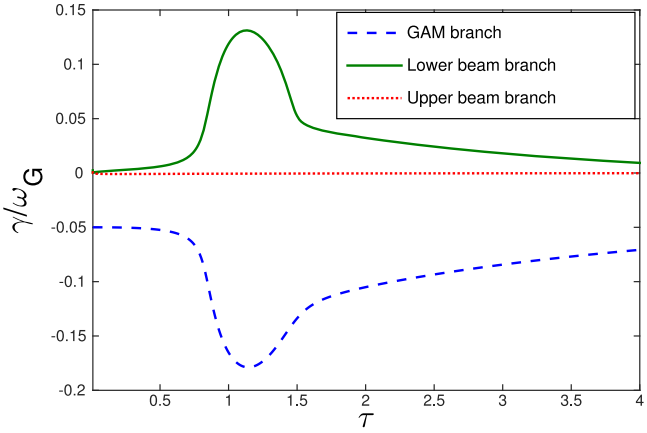

Figure 5. (Reproduced from figure 2 of [84].) Growth rate for $\Lambda_0 B_0 > 2/5$.

experimental results obtained from devices with similar features, for example EAST [91].

3.1.3. Fast EGAM onset due to sharp gradient in pitch angle induced by prompt loss. In DIII-D experiments, EGAM was excited by tangential NBI with relatively large pitch angle [29], and EGAM was observed in less than a millisecond after the turn-on of NBI [77]. A new mechanism was then proposed to explain the fast excitation based on the prompt loss induced sharp gradient in pitch angle, which can explain why modes were often observed during counter-injection [77]. Here, the main steps of the theory will be briefly summarized, while interested readers may refer to the original paper [77] for detailed derivations.

In [77], the EPs were generated by NBI with a single injection velocity u_0 and pitch angle Λ narrowly localized around Λ_0. After one transit/bounce time, the unconfined barely trapped particles with Λ $B_0 \sim 1$ were lost, leaving a sharp gradient in the pitch angle, and the effective EP distribution could be modeled as

$$F_{0,h} = St\frac{\delta(u-u_0)}{u_0^2}\frac{3}{8\pi\Delta\Lambda}\left(1-\left(\frac{\Lambda-\Lambda_0}{\Delta\Lambda}\right)^2\right) \times \Theta(\Lambda-\Lambda_0+\Delta\Lambda)\Theta(\Lambda_0-\Lambda+\Delta\Lambda)\Theta(\Lambda-\Lambda_c), \quad (24)$$

with the pitch angle $\Lambda \equiv u_\parallel/u$, used only in this subsection to be consistent with the original paper, $\Delta\Lambda$ denoting the spreading of pitch angle, Λ_c is the loss boundary, and $\Lambda_0 - \Delta\Lambda < \Lambda_c < \Lambda_0 + \Delta\Lambda$. Furthermore, S is the NBI particle flux and St is the EP density.

Noting that $\partial_E|_\mu F_{0,h} = (\partial_E|_\Lambda + (\partial_E\Lambda)\partial_\Lambda|_E)F_{0,h}$, the sharp gradient at Λ_c may induce strong EGAM drive, and the time needed for the building up of the sharp gradient is of order $\sim\omega_{tr,h}^{-1}$, i.e., one transit/bounce period of the barely trapped EPs. In [77], the EGAM dispersion relation was derived, and solved perturbatively for the beam mode [43, 77]. It was found that, with the existence of sharp gradient, the EGAM onset time was very short, and can be applied to interpret the DIII-D results [29]. The drive was strongest as $\Lambda_0 = \Lambda_c$, i.e., the NBI was maximized at the loss boundary, producing an EP density maximized at the discontinuity of the distribution function.

In the treatment of [77], however, the GAM Landau damping or other possible dissipation channels are missing, which is usually not important for EGAM local instabilities with a given EP density, since GAM Landau damping can be weak compared to the EP resonant drive. However, in the case considered here for the 'fast onset' of EGAMs with EPs density accumulating with time, a finite dissipation may induce a finite threshold on EP density (n_{cr}), and it takes $\tau_c \sim n_{cr}/S$ for the EP density to accumulate. For EGAM with a finite linear growth rate as EP density is above the threshold of marginal instability, the onset time will be $\max(\tau_c, 1/\gamma_L)$ with γ_L being the obtained EGAM linear growth rate.

Besides the cases reviewed above [43, 76, 77, 82, 84], other EP equilibrium distributions were considered, including bump-on-tail [78, 80, 81, 92], and a careful examination of beam versus GAM branch was carried out [78, 80]. Corrections to EGAM local dispersion relation due to electromagnetic effects [93], kinetic electrons [64, 94] and toroidal rotation [95], were also investigated. Readers interested in these works may refer to the original papers for more details.

3.2. Global theory

EGAM may have a global mode structure due to the coupling to GAM continuum, and the nonlocal properties of EGAM are determined by the relative orderings of two scale lengths, i.e., the characteristic scale length of GAM continuous spectrum $L_G \equiv |\omega_G^2(r)/(\partial\omega_G^2(r)/\partial r)|$ and the scale length of EP density profile $L_E \equiv |n_{0,h}(r)/(\partial n_{0,h}/\partial r)|$.

In the absence of GAM continuum, EGAM can be self-trapped by EP density profile, and form a radial EGAM

eigenstate [43, 87] with a radial scale length of $\sqrt{\rho_{d,h}L_E}$, as we will discuss in section 3.2.1. Noting that the EGAM frequency can be significantly lower than local GAM frequency due to non-resonant EP effects [43, 76], the EGAM coupling to GAM continuum can be minimized by localizing the driving EP beam away from where EGAM frequency matches the local GAM frequency, given $L_E \ll L_G$ [43]. In this limit, the exponentially small tunneling coupling to KGAM will lead to a threshold condition on EGAM excitation [43]. However, for more realistic cases with L_E comparable to L_G, the EGAM will strongly couple to GAM continuum [42], leading to a higher threshold on EGAM excitation [44]. In this subsection, the global feature of EGAM will be discussed, for different L_E/L_G such that EGAM coupling to GAM continuum are, respectively, vanishing ($L_E/L_G = 0$), weak ($L_E/L_G \ll 1$) and strong ($L_E/L_G \sim O(1)$).

3.2.1. Radially localized EP drive: EGAM radial eigenstate. We start with EGAM excitation by a radially localized EP beam in uniform thermal plasmas. To account for the global features, kinetic effects should be included to obtain the global mode equation, and the EP FOW effects dominate. Noting that $k_r = -\mathrm{i}\partial_r$, the EGAM mode equation can be written as

$$\left[\frac{\partial}{\partial r}\left(-\frac{1}{2}\rho_{d,b}^2 N_b(r) H\right)\frac{\partial}{\partial r} + \mathscr{E}_{\mathrm{EGAM}}(r)\right]\delta E = 0, \qquad (25)$$

with $H \sim O(1)$ due to EP FOW effects, and its expression given in equation (21) of [43], and $\rho_{d,b} = \rho_{d,h}(E_b, \Lambda_0)$. The characteristic scale length of the mode is $\Delta \simeq \sqrt{\rho_{d,b}L_E} \ll L_E$ to be shown *a posteriori*. Expanding $N_b(r) \simeq N_b(r_0)(1 - (r - r_b)^2/L_E^2)$ and introducing $r - r_b = \xi z$, the mode equation becomes

$$\left[\frac{\partial^2}{\partial z^2} + 2\xi^2\left[-\frac{\mathscr{E}_{\mathrm{EGAM}}(r_b)}{\rho_{d,b}^2 N_b(r_b) H}\right] - z^2\right]\delta E = 0, \qquad (26)$$

where $\xi^4 = \rho_{d,b}^2 N_b(r_b) H L_E^2 \big/ (2(-1 + \omega_G^2(r_b)\big/\omega^2))$ and causality constraint must be applied in determining ξ^2. Equation (26) is the typical Weber equation and its eigenvalues satisfy the following 'localized' EGAM dispersion relation (i.e., neglecting the coupling to the GAM continuum)

$$2\xi^2\left[-\frac{\mathscr{E}_{\mathrm{EGAM}}(r_b)}{\rho_{d,b}^2 N_b(r_b) H}\right] = 2l + 1, \quad l = 0, 1, 2, \ldots. \qquad (27)$$

Here, l is the radial eigenmode number. Meanwhile, the radial electric field is

$$\delta E \propto H_l((r - r_b)/\xi)\exp(-(r - r_b)^2/(2\xi^2)), \qquad (28)$$

with H_l being the lth Hermite polynomial. The ground state with $l = 0$ is the most unstable mode with the straightforward interpretation as the mode structure localized at strongest EP drive.

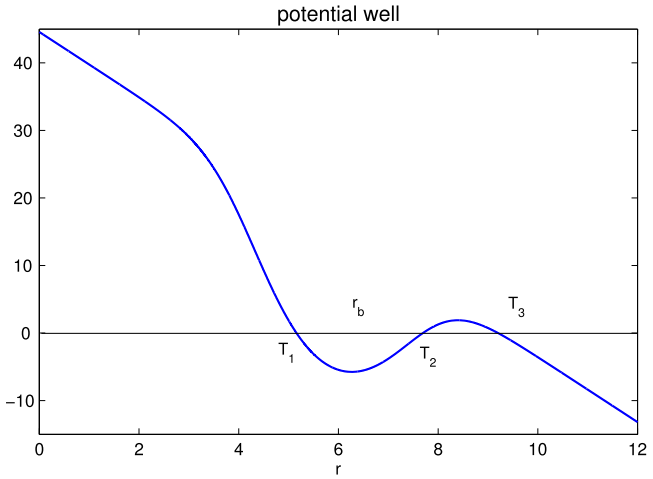

Figure 6. (Reproduced from figure 2 of [43].) Potential well: $-Q$ versus r/L_b.

3.2.2. Radially localized EP drive: weak tunneling coupling to GAM continuum. Considering weak but finite thermal temperature gradient with $L_G \gg L_E$, the EGAM can be coupled to GAM continuum at the point the EGAM frequency matches the local GAM frequency, and the coupling is weak since EGAM mode amplitude is exponentially small at the resonance point. Note that, although thermal ion FLR/FOW is formally much smaller than EP FOW, kinetic effect is dominated by thermal ion FLR as EP density diminishes. Noting that the typical scale length of EGAM is $L \simeq \sqrt{\rho_{d,b}L_E} \ll L_E, L_G$, the mode equation can be written as

$$[\partial_r^2 + Q(r)]\delta E = 0, \qquad (29)$$

with $-Q(r) = 2\mathscr{E}_{\mathrm{EGAM}}(r)\big/(\rho_{d,b}^2 N_b(r) H + \rho_{ti}^2 G)$ being the potential well. The kinetic dispersiveness amplitude is given by $\rho_{d,b}^2 N_b(r) H + \rho_{ti}^2 G$, with the first term due to EP FOW while the second term accounts for thermal ion FLR/FOW, and the expression of G was given in [43] (equation (31) therein). In the EP localization region, kinetic dispersiveness is dominated by EP FOW, and we recover equation (25); while, as EP fade away, equation (29) reduces to that describing KGAM propagation:

$$[\partial_r^2 + 2(1 - \omega_G^2(r)/\omega^2)\big/(\rho_{ti}^2 G)]\delta E = 0, \qquad (30)$$

and the KGAM radial electric field exhibits the characteristic Airy scale $k_r \sim O(\rho_{ti}^{2/3} L_G^{1/3})$. The potential well, $-Q(r)$, is given by figure 6, with three regular turning points (zeros), T_1, T_2 and T_3. T_1 and T_2 are the turning points pair due to the localization effect of EPs, and form a bound state as we have discussed for equation (25). T_3 is the turning point accounting for mode conversion to KGAM, beyond which the mode

propagates outward, as noted in the discussion following equation (30).

Away from the turning points, $Q(r)$ is slowly varying and equation (29) can be solved using WKB approach. In particular, we obtain

$$\delta E = \frac{1}{Q^{1/4}(r)}\Big[A_1 \exp(\mathrm{i}\int \sqrt{Q(r)}\,\mathrm{d}r) + B_1 \exp(-\mathrm{i}\int \sqrt{Q(r)}\,\mathrm{d}r)\Big]. \tag{31}$$

The corresponding WKB dispersion relation of the eigenmode described by equation (29) can then be straightforwardly derived via asymptotic matching of the WKB solutions, equation (31), across the turning points and is given by

$$\mathrm{e}^{2\mathrm{i}W_1} = (\mathrm{e}^{2\mathrm{i}W_2} + 1)/(\mathrm{e}^{2\mathrm{i}W_2} - 1); \tag{32}$$

where $W_1 = \int_{T_1}^{T_2} \sqrt{Q(r)}\,\mathrm{d}r$ and $W_2 = \int_{T_2}^{T_3} \sqrt{Q(r)}\,\mathrm{d}r$. The tunneling coefficient $\mathrm{e}^{2\mathrm{i}W_2}$ is formally exponentially small, and the WKB eigenmode dispersion relation of EGAM becomes approximately

$$W_1 = (l + 1/2)\pi - \mathrm{i}\mathrm{e}^{2\mathrm{i}W_2}, \qquad l = 0, 1, 2, \ldots . \tag{33}$$

Equation (33) is the well-known Bohr–Sommerfeld quantization condition including the tunneling coupling to outgoing KGAM. Neglecting the tunneling coupling in the $L_E/L_G \to \infty$ limit, equation (33) is equivalent to equation (26). Near marginal stability, the global EGAM growth rate can be obtained from the imaginary part of equation (33)

$$\gamma = -W_{1\mathrm{i}}/(\partial W_{1r}/\partial\omega_r) - \mathrm{e}^{2\mathrm{i}W_2}/(\partial W_{1r}/\partial\omega_r); \tag{34}$$

expressing the mode excitation when the EP resonant drive exceeds the tunneling-convective damping, and ω_r is solved from $W_{1r}(\omega_r) = 0$, where W_{1r} and $W_{1\mathrm{i}}$ are, respectively, the real and imaginary parts of W_1 [43]. The mode structure of EGAM from numerical solution of equation (29) (see figure 7) shows mode trapping by localized EP drive with an exponentially small tunneling of the electric field to an outward propagating KGAM due to coupling to GAM continuous spectrum, and it is very similar to the DIII-D observations by Nazikian *et al* [33]. Meanwhile, the EGAM threshold condition, due to non-local coupling to KGAM, is expected to increase for decreasing L_G, and is shown numerically in figure 8 for $L_G = L_1,\ L_2,\ L_3$ with $L_3 < L_2 < L_1 = \infty$.

3.2.3. Radially broad EP drive: strongly coupling to GAM continuum. It is shown in figures 7 and 8 that, the EGAM coupling to GAM continuum increases as its mode radial width $\propto\sqrt{\rho_{d,h}L_E}$ increases with respect to L_G. In realistic tokamak plasmas, it is expected that the EP density profile scale length L_E is comparable to L_G and, thus, the excited EGAM is expected to be strongly dependent on the radial mode structure determined by both radial profiles of EP drive and GAM continuum. As a result, the normalized EP drift

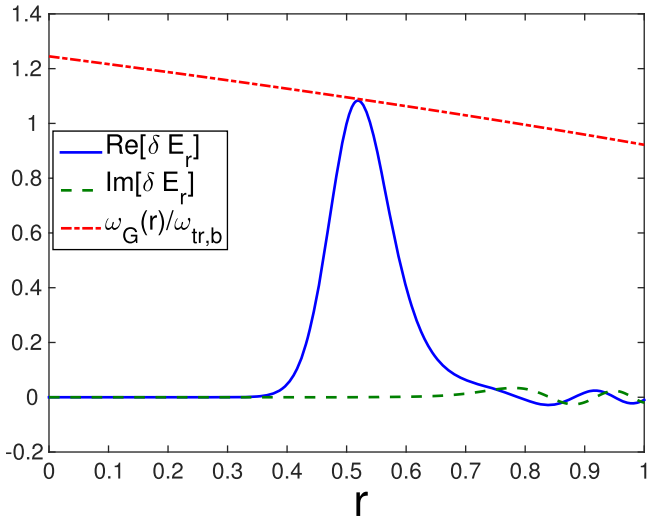

Figure 7. (Reproduced from figure 4 of [43].) Sharply distributed EP: global mode structure.

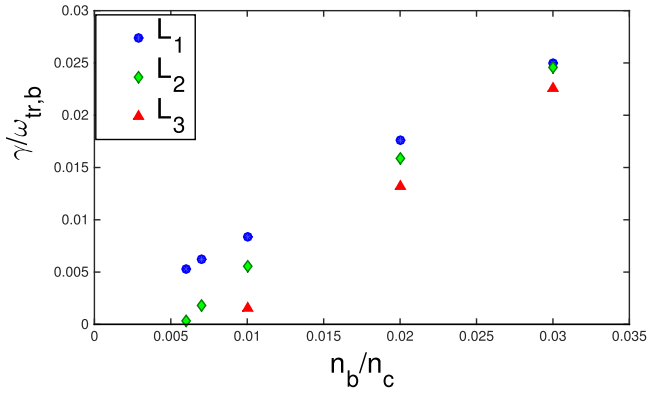

Figure 8. (Reproduced from figure 3 of [43].) Sharply distributed EP: EGAM excitation threshold increases with decreasing L_G.

orbit, $k_r\rho_{d,h}$, changes continuously due to the change of k_r. Away from the singular point, EGAM is characterized by regular radial structure, with $k_r\rho_{d,h} \simeq \sqrt{\rho_{d,h}/L_E} \ll 1$, as we discussed in sections 3.2.1 and 3.2.2. At the resonant coupling position to GAM continuum, however, the mode structure is characterized by $k_r \sim \rho_{ti}^{-2/3}L_G^{-1/3}$, considering the singularity is removed by thermal ion FLR effects, and EPs respond adiabatically to the mode ($|k_r\rho_{d,h}| \gg 1$). In between the regular region and singular layer, the EGAM wavelength varies continuously, and the EGAM eigenmode equation is an integral-differential equation, which generally requires numerical solution.

In [44], the EP response is modeled by Padé approximation, which recovers the EP response at $k_r\rho_{d,h} \ll 1$ and $k_r\rho_{d,h} \gg 1$ limit, and varies continuously with $k_r\rho_{d,h}$:

$$\overline{\delta n_h} = \frac{e}{m}\frac{n_c N_b \overline{\delta\phi}}{\Omega_i^2}k_r^2 \frac{\mathscr{E}_{h0} + Hk_r^2\rho_{d,b}^2/2}{1 + k_r^4\rho_{d,b}^2 n_c N_b H/(2n_E\delta\mathscr{E}_h)} \equiv \frac{e}{m}\frac{n_c N_b \overline{\delta\phi}}{\Omega_i^2}k_r^2\,\mathscr{V}(k_r). \tag{35}$$

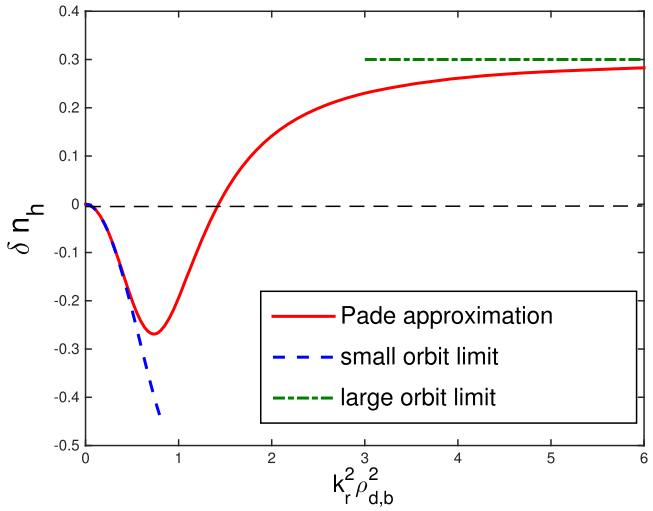

Figure 9. (Reproduced from figure 1 of [44].) Padé approximation surface averaged perturbed EP density. In which, the solid curve is the Padé approximation of the EP response, while the dashed and the dotted–dashed curves are the small and large drift orbit widths responses, respectively.

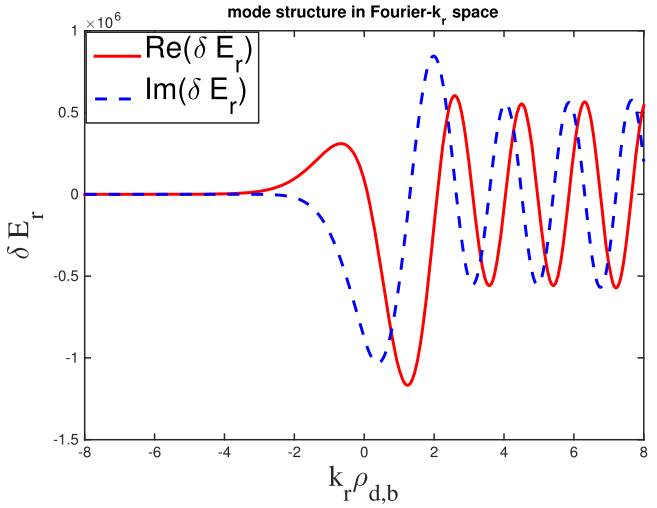

Figure 10. (Reproduced from figure 2 (left panel) of [44].) EGAM eigenmode structure in Fourier-k_r space with $L_G/L_E = 3.5$. The solid and dashed curves are respectively the real and imaginary part of the perturbed radial electric field.

Therefore, this Padé approximation EP response, as shown in figure 9, asymptotically captures the EP response as $k_r\rho_{d,h}$ varies. We note, here, that the equivalent potential function $\mathscr{V}(k_r)$ is independent of r.

Taking a linear radial dependence of the GAM dielectric function, $\mathscr{E}_c \simeq \mathscr{E}_{c0}(1-(r-r_0)/L_G)$, and assuming a Lorentian distribution for the EP radial density profile, $n_E(r) = n_E(r_0)/(1+(r-r_0)^2/L_E^2)$, the EGAM eigenmode equation is reduced to a third order differential equation in the Fourier space, i.e.,

$$\left[\left(\frac{\mathrm{i}}{L_G}\frac{\partial}{\partial k_r}-1\right)\left(\frac{\partial^2}{L_E^2\partial k_r^2}-1\right) + \frac{N_b(r_0)}{\mathscr{E}_{c0}}\mathscr{V}(k_r)\right]\delta E_r = 0. \tag{36}$$

Note that, in equation (36), kinetic effects associated with thermal ion FLR are neglected by taking $G = 0$ since the mode equation in Fourier-k_r space is regular; consequently, the contribution of GAM continuum in the reduced equation on EGAM excitation is continuum damping instead of mode conversion [96].

As $|k_r\rho_{d,h}| \to \infty$, $\mathscr{V}(k_r)$ vanishes as $O(1/k_r^2)$, and equation (36) has the following (out-going wave) boundary condition:

$$\delta E_r(k_r \to +\infty) = \hat{A}\exp(-L_E k_r) + \hat{B}\exp(-iL_G k_r),$$
$$\delta E_r(k_r \to -\infty) = \hat{C}\exp(L_E k_r),$$

with the two exponentially decay terms reflecting the fact that EGAM cannot be effectively driven at small radial scales with $k_r\rho_{d,h} \gg 1$; while the $\exp(-\mathrm{i}L_G\mathrm{k}_r)$ term, with a positive (outward) 'group velocity' in Fourier space, corresponds to generation of singular radial mode structures at the resonant point with GAM continuum and resulting into finite continuum damping. If the thermal ion FLR/FOW effect is properly taken into account, it creates an additional potential well [96] and prevents the mode structure in Fourier space to propagate into regions with $|k_r| \gg \rho_{ti}^{-2/3}L_G^{-1/3}$. This effect, of course, corresponds to resolving the singularity in real space and describes thus, mode conversion to KGAM [12, 49] due to thermal ion FLR effects.

The analytic dispersion relation of the reduced Padé EGAM eigenmode equation, equation (36), can be formally derived via a variational principle. Multiplying δE_r^* to equation (36), subtracting its complex conjugate, and integrating over the Fourier space, we then get the formal dispersion relation of the global EGAM:

$$\gamma\int_{-\infty}^{\infty} N_b(r_0)\frac{\partial \mathrm{Re}(\mathscr{V}(k_r)/\mathscr{E}_{c0})}{\partial\omega_r}|\delta E_r|^2\mathrm{d}k_r = -\int_{-\infty}^{\infty} N_b(r_0)\mathrm{Im}\left(\frac{\mathscr{V}(k_r)}{\mathscr{E}_{c0}}\right)|\delta E_r|^2\mathrm{d}k_r + \frac{(L_G^2+L_E^2)\hat{B}^2}{2L_GL_E^2}. \tag{37}$$

In equation (37), the left hand side represents the rate of change of the total energy and γ is the imaginary part of eigenmode frequency ω. On the right hand side (rhs), the first term represents the EP resonant drive, while the second term represents dissipation due to generation of short wavelength structures, i.e., continuum damping; and '$\hat{B}$' corresponds to the ratio of the mode amplitude at the resonant point compared to that at the center of EP localization region, and is to be determined from numerical solution of the reduced EGAM eigenmode equation. Thus, equation (37) is exactly the Fourier space counterpart of equation (11) of [42], describing the EGAM excitation as EP drive in the ideal region exceeds the threshold due to continuum damping in the inertial layer, analogous to the well studied EPM problem, including fishbone [30, 97–99].

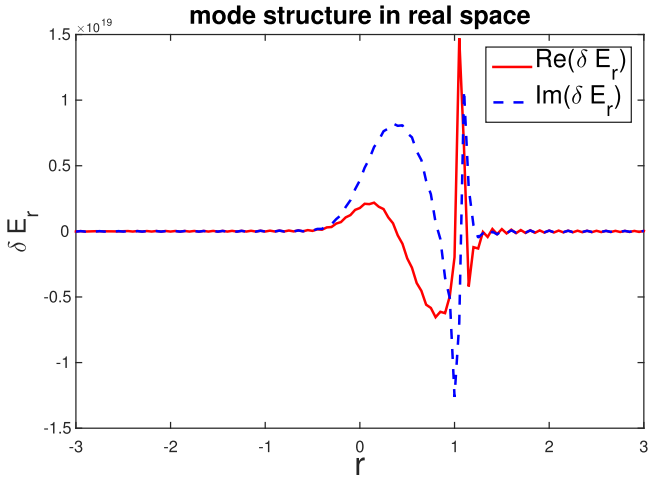

Figure 11. (Reproduced from figure 2 (right panel) of [44].) EGAM eigenmode structure in real space of the same case as figure 10.

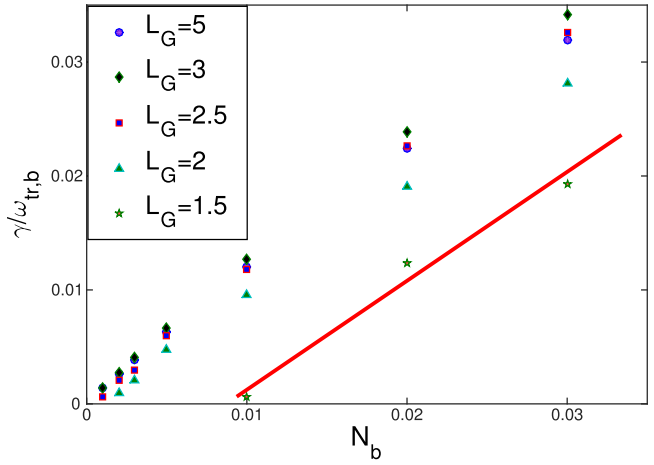

Figure 12. (Reproduced from figure 3 of [44].) Dependence of EGAM growth rate on normalized EP density for different L_G/L_E. The solid line is a linear fitting of the stars corresponding to $L_G/L_E = 1.5$.

Equation (36) is solved using a shooting code, and the obtained structure of the most unstable mode is given in figure 10, which is localized at small k_r with a long tail to large k_r. Note that, although figure 10 looks very similar to figure 7 for localized EP drive, physics picture is in fact very different. Figure 7 is the real space mode structure in the $L_E/L_G \ll 1$ limit, and the long tail corresponds to mode conversion to KGAM due to thermal ion FLR effects at the point EP density becomes vanishingly small. Figure 10, meanwhile, shows the Fourier space mode structure in the $L_E/L_G \sim O(1)$ limit, and the long tail corresponds to singular mode structure due to coupling to GAM continuum where EP density is finite, and thermal ion FLR effect is neglected. By Fourier transformation of fluctuation structures in figure 10, the corresponding mode structure in real space is given in figure 11, and the significant difference with respect to figure 7 becomes obvious. The increasing threshold on EP density due to strong coupling to GAM continuum is shown in figure 12, as we have anticipated.

Note that, in [44], the Padé approximation of EP response captures the feature of EP drive dependence on EGAM radial wavenumber, while the resonant drive is from the primary transit resonance $\omega = \pm\omega_{tr,h}$. This is qualitatively valid since the global mode structure is emphasized here. As we discussed in section 2.2, in the short wavelength limit with $k_r\rho_d \sim O(1)$, higher order transit harmonic resonances will also contribute and significantly increase wave–particle energy exchanges [39, 45, 57, 58, 64]. It would be interesting to have the general integral-differential equation with realistic EP response given as equation (19) solved numerically, and compared to the results based on the Padé approximation of EP response discussed here.

3.3. Nonlinear EGAM saturation and EP transport

The nonlinear dynamics of EGAM can be understood using the analogy of EGAM with the one dimensional BPI, as we discussed in section 3.1.1. The nonlinear evolution of EGAM, due to the nonlinear interactions with EPs, can be obtained from equation (17), with the perturbed EP response derived from equation (20) and the evolution of the 'equilibrium' EP distribution function, $F_{0,h}$, due to nonlinear interactions with EGAM properly taken into account. The $F_{0,h}$ evolution due to nonlinear interaction with EGAM, can be shown to obey the following Dyson equation [4, 86, 100]

$$\bar{\omega}\hat{F}_{0,h}(\bar{\omega}) = -\frac{e^2\hat{\omega}_{dr}}{16}|\delta\phi_G|^2\frac{\partial}{\partial E}\left[\frac{\hat{\omega}_{dr}(\bar{\omega}-\mathrm{i}\gamma)}{(\bar{\omega}-\mathrm{i}\gamma)^2-(\omega_{0r}^2-\omega_{tr})^2}\right] \times \frac{\partial}{\partial E}\hat{F}_{0,h}(\bar{\omega}-2\mathrm{i}\gamma) + \mathrm{i}F_{0,h}(0). \tag{38}$$

Here, $\hat{F}_{0,h}$ is the Laplace transform of $F_{0,h}$, $\bar{\omega}$ denotes the slow nonlinear time scale for $F_{0,h}$ evolution from its initial value $F_{0,h}(0)$, and $|\gamma| \ll \omega_{0r}$ is the growth rate of $\delta\phi_G$. Equation (38) is of the form of a Dyson equation, and describes the evolution of $F_{0,h}$, due to emission and reabsorption of a single coherent EGAM. Note that, in deriving equation (38), only evolution in E needs to be taken into account [38], since both P_ϕ and μ are conserved for EGAM with $n = 0$ and $\omega_G \ll \Omega_{ci}$.

The EGAM equation with the slowly temporal evolving EP 'equilibrium' distribution function obtained from equation (38) then describes the evolution of EGAM due to the self-consistent nonlinear interactions of EPs, and exhibits various physics such as wave–particle trapping [38, 90, 101], hole and clump pair formation [79, 102] and phase-space ZS generation and frequency chirping [4, 98]. This topic is subject of ongoing research, and an exhaustive analysis is beyond the scope of the present brief review. As illustration and example of nonlinear behavior and particle transport in phase space, we will briefly introduce the wave–particle trapping in the weak drive limit. We will also qualitatively discuss the secular dynamics in the strong drive limit.

In the weak drive limit, EGAM saturation due to the wave–particle trapping can be demonstrated using test particle approach; with resonant EP orbit only slightly modified. For simplicity, we consider the $T_e/T_i \ll 1$ case, and EGAM is

characterized by radial electric field only. Noting that wave–particle energy exchange, is induced by the particle radial acceleration associated with the radial magnetic drift $\dot{E} = (e/m)\mathbf{V}_d \cdot \delta\mathbf{E}_r$ and $\dot{\mathbf{R}} = v_\parallel \mathbf{b} + \mathbf{V}_d + \delta\mathbf{V}_E$, with $\delta\mathbf{V}_E$ being the $\mathbf{E} \times \mathbf{B}$ drift induced by radial GAM electric field, one then has

$$\dot{v}_\parallel = \frac{e}{2mv_\parallel}\hat{V}_{\rm dc}\delta E_r \sin\Theta,$$

where $\Theta = \theta - \omega t + k_G r$ is the phase of resonant particles in the slowly varying wave frame, and $\hat{V}_{\rm dc} = v_\parallel^2/(\Omega R_0)$ is the magnetic curvature drift. Noting that, $\dot{\Theta} = \dot{\theta} - \omega + k_G \dot{r}$, with $\dot{\theta} = \omega_{tr} + \delta V_E/r$, and averaging over fast varying scales, one obtains

$$\ddot{\Theta} = \frac{e}{2mv_\parallel qR_0}\hat{V}_{\rm dc}\delta E_r \sin\Theta. \tag{39}$$

This is the typical pendulum equation [101, 103, 104], describing the resonant EP being trapped by and exchanging energy with EGAM. When the wave–particle trapping frequency, $\omega_B \equiv \sqrt{e\hat{V}_{\rm dc}\delta E_r/(2m_i v_{\parallel,\rm res} qR_0)}$ is comparable to the EGAM linear growth rate, the mode enters the nonlinear dynamics phase and eventually saturate; as shown by numerical simulations [78, 90]. In this limit, the resonant EP trajectory is only slightly modified with respect to its equilibrium orbit due to pitch angle scattering, and the drift orbit center position is unchanged; as a result, there is no EP loss.

In the strong drive limit, however, EP loss may be induced by pitch angle scattering [29]. EGAM self-consistent evolution can be understood in analogy with the secular fishbone paradigm [4, 97, 105–108]. Taking well-circulating EPs as example, the nonlinear evolution of EGAM dominated by nonlinear phase-locking [4] can be qualitatively speculated as follows: resonant EP parallel velocity, and thus, EP transit frequency decreases as it passes energy to EGAM through transit resonance; and EGAM frequency dominated by EP characteristic frequency decreases consequently. The frequency downward chirped EGAM can keep in phase with EPs losing energy, leading to nonadiabatic EGAM downward frequency chirping and resonant EP phase space structure secular evolution towards magnetically trapped particle boundary, similar to the 'wave–particle pumping' of fishbones [105]. EPs are lost as they pass the trapped-passing boundary, and become barely trapped particles with unconfined banana orbits, characterized by radial width comparable with torus minor radius. This subject is topic of ongoing research, and will be presented in a future publication.

4. Nonlinear GAM excitation by DWs

The ultimate interest of the fusion community in GAMs is motivated by its potential interactions with DWs/DAWs and thus, by its positive effect in regulating turbulences and transport [12, 26, 109, 110]. This is achieved via spontaneous excitation of GAM by DWs turbulences, and by scattering of the driving DWs into stable short radial wavelength domain. The nonlinear excitation of GAM by DWs can be described by a parametric decay instability [111, 112], where pump DW resonantly decay into a GAM and another DW. GAM nonlinear excitation by DW has been investigated by analytical theory [12, 46, 113–119], numerical simulation [120–127]. The underlying three-wave interactions has also been observed experimentally [23, 128–130]. In section 4, we will briefly review these nonlinear wave–wave interactions in the gyrokinetic theoretical framework, and emphasize the effects of kinetic dispersiveness and mode structure associated with realistic geometry and system nonuniformity; which can all affect the nonlinear GAM excitation process qualitatively. As a result, to quantitatively understand and predict fluctuation induced transport, kinetic treatment and realistic geometry must be properly accounted for.

4.1. Theoretical model

We start with the nonlinear excitation of GAM by DW turbulence. The corresponding gyrokinetic theory was first presented in [12], while the detailed derivation was given later in [46]. Kinetic treatment is needed here, since the nonlinear coupling increases with increasing $|k_\perp \rho_{ti}|$ [12] while the kinetic dispersiveness associated with finite $k_\perp \rho_{ti}$ would significantly affect the nonlinear cross-section [46, 131]. The nonlinear equations for the GAM-DW system can be obtained from the quasineutrality condition, with the nonadiabatic particle response derived from nonlinear gyrokinetic equation [52]. Separating the linear and nonlinear response as $\delta H \equiv \delta H^L + \delta H^{\rm NL}$, and applying the $\omega \gg \omega_{tr,i}, \omega_{d,i}$ assumptions while solving for the nonlinear ion responses, one then obtains [132],

$$\begin{aligned}\frac{n_0 e^2}{T_i}\left(1 + \frac{T_i}{T_e}\right)\delta\phi_k - \langle eJ_k \delta H_i^L\rangle_k + \langle e\delta H_e^L\rangle_k \\ = -\frac{\rm i}{\omega_k}\langle e\Lambda^{\mathbf{k}}_{\mathbf{k}',\mathbf{k}''}\delta\phi_{k'}\delta H_{e,k''}\rangle_k \\ - \frac{\rm i}{\omega_k}\langle e\Lambda^{\mathbf{k}}_{\mathbf{k}',\mathbf{k}''}(J_k J_{k'} - J_{k''})\delta\phi_{k'}\delta H_{i,k''}\rangle_k.\end{aligned} \tag{40}$$

The first term on the rhs of equation (40) is formally $O(1/(k_\perp^2\rho_{ti}^2))$ larger than the second term from polarization nonlinearity [133], for modes with $k_\perp \rho_{ti} \ll 1$. However, for the nonlinear GAM equation, the contribution from the first term vanishes due to $\delta H_{d,e} = 0$, and the nonlinear GAM equation, then becomes

$$\begin{aligned}\frac{n_0 e^2}{T_i}\left(1 + \frac{T_i}{T_e}\right)\delta\phi_G - \langle eJ_G \delta H_i^L\rangle_G + \langle e\delta H_e^L\rangle_G \\ = -\frac{\rm i}{\omega_G}\langle e\Lambda^{\mathbf{k}}_{\mathbf{k}',\mathbf{k}''}(J_{k'} - J_{k''}) \\ \times (\delta\phi_{k'}\delta H_{i,k''} + \delta\phi_{k''}\delta H_{i,k'})\rangle_G.\end{aligned} \tag{41}$$

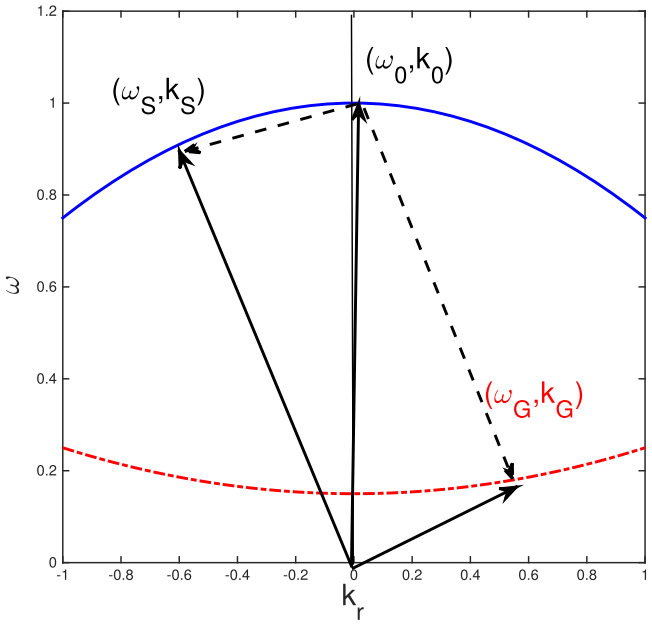

Figure 13. Parametric decay of a pump DW into a GAM and a DW lower sideband.

On the other hand, for nonlinear DW equation, noting that $\delta H_{d,e} = 0$ while $\delta H_{G,e} \neq 0$, there is no commutative cancellation in the first term on the rhs of equation (40), and the DW equation reduces to

$$\frac{n_0 e^2}{T_i}\left(1 + \frac{T_i}{T_e}\right)\delta\phi_k - \langle eJ_k \delta H_i^L\rangle_k = e\frac{c}{B}\frac{1}{\omega_k}k'_\theta \delta\phi_{k'}\frac{\partial\langle\delta H_{e,G}\rangle}{\partial r}, \quad (42)$$

with the selection rule $\mathbf{k} = \mathbf{k}' + \mathbf{k}_G$.

Note that equations (41) and (42) are derived using the $k_\perp\rho_{ti} \ll 1$ and $1/q \ll 1$ expansions, while no assumptions on the mode amplitudes are made except the gyrokinetic ordering [52]. As a result, equations (41) and (42) are general, and can be applied to study the nonlinear saturation of DWs [74, 134, 135]. In this paper, for the sake of simplicity, we will only review the results obtained for the 'linear' growing stage of the parametric instability, with the emphasis on the effect of system nonuniformities and kinetic dispersiveness on GAM excitation. The nonlinear dynamics of the coupled DW-GAM system including saturation is beyond the scope of this review and, in fact, it is still under active investigation.

Consistent with the linear growth stage of the parametric instability of interest, through out section 4, we separate the DW into a pump $\Omega_0(\omega_0, \mathbf{k}_0)$ with finite and fixed amplitude and its lower sideband $\Omega_S(\omega_S, \mathbf{k}_S)$ with much smaller intensity. Thus, we investigate the resonant decay of the pump DW into a GAM $\Omega_G(\omega_G, \mathbf{k}_G)$ and the lower sideband; while the feedback of the two daughter waves, i.e., Ω_G and Ω_S, on the pump DW, playing important role in the spectrum evolution and transport, is beyond the scope of this work. Note that, compared to ZFZF generation by DWs [26, 132, 136, 137], where nonlinear interactions with both lower and upper DW sidebands are considered, only the lower DW sideband satisfying the resonant decay condition is considered here, as shown in figure 13. The governing nonlinear equations can be derived from equations (41) and (42), taking $\delta\phi_d = \delta\phi_P + \delta\phi_S$, with the ballooning mode decomposition for $\delta\phi_d$:

$$\delta\phi_P = A_P e^{-in\xi - i\omega_P t}\sum_m e^{im\theta}\Phi_0(nq - m) + \text{c.c.},$$
$$\delta\phi_S = A_S e^{in\xi - i(\omega_G - \omega_P)t}\sum_m e^{-im\theta}\Phi_0^*(nq - m) + \text{c.c.},$$
$$\delta\phi_G = A_G e^{-i\omega_G t} + \text{c.c.};$$

and the eikonal Ansatz for the radial envelopes; i.e.,

$$A_P = e^{i\int k_P dr},$$
$$A_S = e^{-i\int k_P dr}(e^{i\int k_G dr} + \text{c.c.}),$$
$$A_G = e^{i\int k_G dr} + \text{c.c.}$$

Here, Φ_0 accounts for the fine radial scale structure due to finite $k_\parallel$ and magnetic shear, with the characteristic radial scale being of the order of the distance between neighboring mode rational surfaces, and the normalization condition $\int_{-\infty}^{\infty}|\Phi_0|^2 dr = 1$ is assumed without loss of generality. One then has

$$D_S\partial_t A_S = -\frac{c}{B}k_{\theta,P}k_{r,G}\frac{T_i}{T_e}A_P^* A_G, \quad (43)$$

$$\mathscr{E}_{\text{GAM}}\partial_t\delta\phi_G = -\alpha_i\frac{c}{2B}k_{\theta,P}k_{r,G}^3\rho_{ti}^2 A_S A_P, \quad (44)$$

with $\mathscr{E}_{\text{GAM}}$ being the linear GAM dielectric dispersion function [12] defined as

$$\mathscr{E}_{\text{GAM}} \equiv 1 + T_i/T_e + T_i(\langle\delta H_e\rangle - \langle J_0\delta H_i\rangle)_G/(en_0\delta\phi_G),$$

$\alpha_i = 1 + \delta P_\perp/(en_0\delta\phi_P)$ being an order unity function of local equilibrium parameters defined in [26], and $D_S \equiv D_P(\omega_S, \mathbf{k}_S, r)$ with D_P the linear DW dispersion function formally defined by

$$D_P \equiv 1 + \frac{T_i}{T_e} - \int_{-\infty}^{\infty}\Phi_0^*\langle eJ_P\delta H_{P,i}^L\rangle dr/\left(\frac{n_0 e^2}{T_i}A_P\right).$$

For DWs with typically quadratic dispersiveness, a model dispersion function can be assumed, i.e., $D_P = \omega - \omega_{*0}\exp(-(r - r_0)^2/L_*^2) + C_d\omega_{*0}\rho_{ti}^2 k_r^2 + iD_I$. ω_{*0} is the diamagnetic drift frequency at the gradient peak (r_0), and the Guassian profile indicates a localized instability drive around gradient peak. We then have

$$D_S = i\partial_t + i\gamma_S - \omega_P + \omega_{*0}\left(1 - \frac{(r - r_0)^2}{L_*^2}\right) + C_d\omega_{*0}\rho_i^2\frac{\partial^2}{\partial r^2}.$$

Defining $\mathscr{E}_G = \partial_r \delta\phi_G/\alpha$, with $\alpha = \mathrm{i}(\alpha_i \omega_P T_e/T_i)^{1/2}$, we obtain the following coupled nonlinear equations [51]:

$$D_S A_S = \mathrm{i}\Gamma_0^* \mathscr{E}_G, \tag{45}$$

$$D_G \mathscr{E}_G = -\Gamma_0 \partial_t \partial_r^2 A_S, \tag{46}$$

in which $\Gamma_0 \equiv (\alpha_i T_i/\omega_P T_e)^{1/2} c k_{\theta,P} A_P/B$ is the normalized pump amplitude, $D_G = (\partial_t^2 + \omega_G^2(r) + 2\mathrm{i}\omega_G\gamma_G - (G/2)\omega_G^2(r_0)\rho_{ti}^2\partial_r^2)$ with the kinetic dispersiveness term (proportional to G) due to FLR/FOW of GAM, and the expression of G can be obtained from equation (14) (or equation (31) of [43]; see also section 3).

Equations (45) and (46) are the coupled nonlinear DW sideband and GAM equations, and describe the nonlinear parametric generation of these spectral components by the fixed amplitude pump DW, while the feedback of GAM and DW sideband on the pump DW is neglected due to the $|\delta\phi_G|, |\delta\phi_S| \ll |\delta\phi_P|$ ordering. Note that there are several different radial scales involved in equations (45) and (46), i.e., the pump DW radial envelope scale L_P, the scale length of diamagnetic drift frequency L_*, and the GAM continuum scale length L_G. Note that we typically have $L_P \sim \sqrt{\rho_{ti} L_*} \ll L_*, L_G$, and the global DW-GAM problem can then be simplified due to spatial scale separation, with system nonuniformities enter at different spatial scales. The local theory for GAM excitation is presented in section 4.2, while the role of system nonuniformities is analyzed in section 4.3. The extension of the present theory, largely based on the $k_\perp\rho_{ti} \ll 1$ expansion, to short wavelengths and its application to CTEM with typically $k_\perp\rho_{ti} \sim O(1)$ is carried out in section 4.2.2. Electromagnetic effects are discussed in section 4.2.3.

4.2. GAM excitation by DWs: local theory

4.2.1. GAM excitation by DWs: parametric dispersion relation. We start from the local limit of the general theory presented in section 4.1, which is discussed in most publications [12, 113–116]. Thus, all the system nonuniformities are neglected, and we focus on the nonlinear interaction strength, defined by the relevant cross-section; i.e., the coefficients of the nonlinear couplings. Furthermore, taking $\partial_t = -\mathrm{i}\omega + \gamma$ and $\partial_r = \mathrm{i}k_r$ in equations (45) and (46), one then has

$$(\gamma + \gamma_S)(\gamma + \gamma_G) = k_G^2 \Gamma_0^2, \tag{47}$$

with γ_S, γ_G being the damping rates of DW sideband and GAM, respectively. In deriving the above local parametric instability dispersion relation, the frequency and wavenumber matching conditions for resonant decay illustrated in figure 13, are applied, i.e.,

$$\omega - \omega_P + \omega_* - C_d \omega_* \rho_{ti}^2 k_G^2 = 0,$$
$$\omega^2 - \omega_G^2 - G\omega_G^2 \rho_{ti}^2 k_G^2/2 = 0,$$

corresponding to energy and momentum conservation in the parametric decay process.

The threshold condition for GAM spontaneous excitation is then given by $k_G^2\Gamma_0^2 = \gamma_S\gamma_G$; while, in the strong drive limit with the pump DW amplitude well above threshold, the GAM growth rate is $\gamma = k_G\Gamma_0$. Note that the nonlinear drive increases with k_G, i.e., the generation of short wavelength KGAM is preferred. This provides the motivation for the kinetic treatment here, especially when the group velocities of DW sideband and GAM, proportional to k_G, are accounted for. This also motivates deriving the short wavelength KGAM dispersion relation, especially the damping rate γ_G in section 2.2 that determines the threshold condition for the parameter regime of practical interest.

Before the discussion of global properties of the parametric instability, we would like to briefly discuss the extensions of the present model, summarized by governing equations (45) and (46) and derived based on the $k_\perp\rho_{ti} \ll 1$ expansion for electrostatic DWs, to short wavelengths $k_\perp\rho_{ti} \sim O(1)$ and its application to CTEM DW [119]. We also generalize our analysis to electromagnetic limit with application to GAM excitation by TAE [138]. These two different cases are described by governing equations with forms similar to equations (45) and (46), despite nonlinear terms have different origin and structure. As a result, the global properties discussed in section 4.3 can be, at least qualitatively, applied to the processes discussed in sections 4.2.2 and 4.2.3.

4.2.2. GAM excitation by short wavelength CTEM. The kinetic theories of GAM excitation by DWs discussed so far are derived based on the small argument expansion of the Bessel functions accounting for FLR effects. This is generally not applicable to CTEM DW [139–142] with typically $k_\perp\rho_{ti} \sim O(1)$. Another major difference of CTEM with ITG lies in the electron kinetic response, which is also expected to affect the nonlinear CTEM dynamics, including the excitation of GAM. The excitation of GAM by CTEM is of interest because GAM is preferentially excited in the plasma edge, where GAM Landau damping rate is minimized due to its dependence q, and where CTEM are also localized due to the fraction of trapped electrons increasing with r/R_0. Numerical simulations using core plasma parameters suggest that GAM excitation is not important for CTEM nonlinear dynamics [143, 144], while possible important role of GAMs in regulating CTEM turbulence is observed in simulations using edge-like parameters [126]. The analytical theory for GAM excitation by CTEM was developed in [119], with emphasis on dominant contributions on nonlinear couplings from ions and electrons in different wavelength regimes.

The corresponding nonlinear GAM equation, with an expression similar to equation (44), can be derived as

$$\mathscr{E}_{\mathrm{GAM}} A_G = \mathrm{i}\frac{c}{B_0} k_G k_\theta \frac{1}{\omega_0^2}(F_1 - \alpha_e) A_P A_S. \tag{48}$$

Here,

$$F_1 = \left\langle J_0 J_S J_G F_0 \frac{\overline{\omega_G \omega_{*,i} + (\omega_0 - \omega_{*,i})\omega_{dr}}}{\omega_G - \omega_{dr}} \right\rangle$$

is due to ion nonlinearity, and

$$\alpha_e \equiv -\frac{T_i}{T_e}B_0\int E\mathrm{d}E\mathrm{d}\Lambda\left|\overline{\overline{\sum_m \mathrm{e}^{(\mathrm{i}(nq-m)\theta)}}}\right|^2 F_0\omega_{*,e}\oint\frac{\mathrm{d}\theta}{v_\parallel}$$

is related to the trapped electron nonlinearity [2, 8, 132], with $\overline{\overline{(\cdots)}}$ denoting bounce averaging. In deriving α_e, only the contribution of electron temperature gradient to $\omega_{*,e}$ is considered.

The CTEM sideband equation, can be derived similarly,

$$D_S A_S = -\mathrm{i}\frac{c}{B_0}k_G k_\theta\frac{1}{\omega_0^2}(F_1-\alpha_e)A_G A_P^*, \tag{49}$$

where $D_S \equiv D_{Ct}(\omega_S, \mathbf{k}_S)$ is the linear dispersion function of CTEM sideband, and

$$D_{Ct}\equiv 1+\frac{T_i}{T_e}-\int_{-\infty}^{\infty}\Phi_0^*[\langle J_0\delta H^L_{Ct,i}\rangle-\langle\delta H^L_{Ct,te}\rangle]\mathrm{d}r \Big/\left(\frac{n_0 e}{T_i}\int_{-\infty}^{\infty}\Phi_0^*\delta\phi_{Ct}\mathrm{d}r\right).$$

Noting $D_S\simeq -\mathrm{i}\partial_{\omega_0}D_{Ct,r}(\gamma+\gamma_S)$, one then obtain the following parametric instability dispersion relation

$$(\gamma+\gamma_G)(\gamma+\gamma_S)=\Gamma^2_{D,Ct}, \tag{50}$$

which is similar to equation (47) derived in the $|k_\perp\rho_{ti}|\ll 1$ long wavelength limit. Here, the nonlinear drive due to both ion and trapped electrons is given by

$$\Gamma^2_{D,Ct}\equiv\left(\frac{c}{B_0}k_\theta\frac{1}{\omega_0^2}\right)^2\frac{\omega_G}{\rho_i^2\partial D_{Ct,r}/\partial\omega_0}(F_1-\alpha_e)^2|A_0|^2.$$

The trapped electron contribution is typically proportional to $\alpha_e/\omega_*\sim O(\sqrt{\epsilon})$, while the ion contribution F_1 is sensitive to the perpendicular wavelength $k_\perp\rho_{ti}$. Thus, ions and trapped electrons contributions dominate in the long and short wavelength limit, respectively. Meanwhile in the general case with $k_\perp\rho_{ti}\sim O(1)$, it can be estimated that F_1 and α_e are both positive in the simple $\eta_i=\eta_e=0$ limit. The contributions from electrons and ions will, therefore, compete with each other, and thus, numerical solution is required for assessing the CTEM parametric decay rate in the general case. This analysis is also of broader interests for the nonlinear dynamics of kinetic Alfvén waves (KAW), e.g., convective cells generation by KAW [145], nonlinear decay of KAW [146] and kinetic TAE [147–149].

4.2.3. GAM excitation by TAE. Alfvénic instabilities excited by EPs, e.g., fusion-αs, are important for burning plasmas, due to their roles in EP as well as thermal plasma transport processes, as reviewed in [98]. Of particular interest is TAE, which exists in the toroidicity induced SAW continuum gap with minimized excitation threshold [150–152]. Nonlinear excitation of ZS is one possible channel for Alfvénic instability nonlinear saturation [153–156]. Spontaneous excitation of GAM by TAE was investigated in [138], demonstrating that the pump TAE is scattered into a TAE sideband with finite radial envelope due to GAM modulation. The main difference in the electromagnetic TAE case, with respect to the electrostatic DW situation discussed above, is the additional contribution from the nonlinear Maxwell stress term, i.e., the $\boldsymbol{\delta J}\times\boldsymbol{\delta B}$ term in momentum equation. For the SAW related instability in ideal MHD uniform plasma limit, Maxwell stress may cancel Reynolds stress, yielding the well-known 'pure Alfvénic state' (PAS), where the Alfvénic fluctuation can exist at finite amplitude without significant distortion from nonlinearity [157]. The generation of ZS, including GAM spontaneous excitation by TAE, is enabled by the breaking of PAS due to, e.g., toroidicity as an intrinsic nonuniformity of tokamak [153].

Nonlinear vorticity equation [158, 159] is needed in addition to the quasi-neutrality condition

$$\begin{aligned}&\frac{c^2}{4\pi\omega^2}B\frac{\partial}{\partial l}\frac{k_\perp^2}{B}\frac{\partial}{\partial l}\delta\psi_k+\frac{e^2}{T_i}\langle(1-J_k^2)F_0\rangle\delta\phi_k\\&-\sum\left\langle\frac{q}{\omega}J_k\omega_d\delta H\right\rangle_k=-\mathrm{i}\frac{c}{B\omega}\sum_{\mathbf{k}=\mathbf{k}'+\mathbf{k}''}\hat{\mathbf{b}}\cdot\mathbf{k}''\times\mathbf{k}'\\&\times\left[\left\langle e(J_kJ_{k'}-J_{k''})\left(\delta\phi+\frac{\mathrm{i}}{\omega}v_\parallel\partial_l\delta\psi\right)_{k'}\delta H_{i,k''}\right\rangle\right.\\&\left.+\frac{k_\perp''^2c^2}{4\pi}\frac{1}{\omega_{k'}\omega_{k''}}\partial_l\delta\psi_{k'}\partial_l\delta\psi_{k''}\right];\end{aligned} \tag{51}$$

with the terms on the left hand side being, respectively, field line bending, inertia and ballooning-interchange terms, and the terms on the rhs being Reynolds and Maxwell stresses. Furthermore, $\delta\psi\equiv\omega\delta A_\parallel/(ck_\parallel)$ is defined as an additional variable, and the ideal MHD parallel Ohm's law is recovered if we take $\delta\phi=\delta\psi$. The particle responses are derived from the nonlinear gyrokinetic equation, equation (10), in the $\beta\ll 1$ limit, while higher order electro-magnetic component of GAM is neglected.

Noting $\delta H^L_{T,e}=-(e/T_e)F_0\delta\phi_T$ and $\delta H^L_{T,i}\simeq(e/T_i)F_0J_T\delta\phi_T$, the GAM equation can be derived from the vorticity equation in the form

$$\omega_G\mathscr{E}_{\mathrm{GAM}}A_G=-\frac{\mathrm{i}}{2}\frac{c}{B}k_{0,\theta}k_G^3\rho_{ti}^2\left(1-\frac{\omega_A^2}{4\omega_0^2}\right)A_SA_0, \tag{52}$$

with $\omega_A\equiv V_A/(qR_0)$, and the two terms in the bracket on the rhs corresponding to, respectively, the Reynolds and Maxwell stresses.

Due to the coupling to GAM, the TAE sideband deviation from ideal MHD can be derived from quasi-neutrality condition

$$\delta\phi=\delta\psi-\mathrm{i}\frac{c}{B}k_{0,\theta}k_G\frac{1}{\omega_0}\delta\phi_G\delta\psi_0^*. \tag{53}$$

Substituting into the vorticity equation, one then obtains the nonlinear TAE sideband eigenmode equation

$$k_{\perp,S}^2\epsilon_{T,S}A_S=2\mathrm{i}\frac{c}{B}k_{0,\theta}k_G\omega_0k_{0,\perp}^2A_0^*A_G, \tag{54}$$

where $\epsilon_{T,S}=\omega_A^4\Lambda_T(\omega_S)D(\omega_S,k_G)/(\epsilon_0\omega_S^2)$, $D(\omega,k_G)=(\Lambda_T(\omega)-\delta\hat{W}(\omega,k_G))$ with $\Lambda_T=\sqrt{-\Gamma_-\Gamma_+}$, $\Gamma_\pm\equiv(\omega^2/\omega_A^2-$

$1/4) \pm \epsilon_0\omega^2/\omega_A^2$ and $\delta\hat{W}(k_G, \omega)$ playing the role of a normalized potential energy [160]. Furthermore, $\epsilon_0 = 2(\epsilon + \Delta')$ with Δ' being the Shafranov shift in the shifted circular magnetic flux surfaces tokamak case we consider here. Solutions of $D(\omega, k_G) = 0$ are $\omega = \omega_T(k_G)$, with the pump TAE frequency given by $\omega_0 = \omega_T(k_G = 0)$.

The nonlinear dispersion relation of the parametric instability can be obtained by combining equations (52) and (54)

$$\mathscr{E}_{\mathrm{GAM}}\epsilon_{T,S} = \left(\frac{c}{B}k_{0,\theta}k_G^2\rho_{ti}\right)^2\frac{k_{0,\perp}^2}{k_{S,\perp}^2}\frac{\omega_0}{\omega_G}\left(1 - \frac{\omega_A^2}{4\omega_0^2}\right)|A_0|^2.$$

The nonlinear excitation then relies on the breaking of PAS $(1 - \omega_A^2/(4\omega_0^2) \neq 0)$ by toroidicity. Noting $D(\omega_S, k_G) \simeq -\mathrm{i}\partial_{\omega_0}D(\gamma + \gamma_S)$, We thus obtain the dispersion relation of the parametric decay process

$$(\gamma + \gamma_S)(\gamma + \gamma_G) = \Gamma_{D,T}^2; \tag{55}$$

where the driving term $\Gamma_{D,T}$ is defined as

$$\Gamma_{D,T}^2 \equiv \left(\frac{c}{B}k_{0,\theta}k_G\right)^2\frac{k_{0,\perp}^2}{k_{S,\perp}^2}\frac{\epsilon_0\omega_0^3}{\omega_A^4\Lambda_T(\omega)} \times \frac{|A_0|^2}{\partial_{\omega_0}D_0}\left(1 - \frac{\omega_A^2}{4\omega_0^2}\right). \tag{56}$$

For typical tokamak parameters, one has $\omega_0\partial_{\omega_0}D_0 > 0$. The spontaneous excitation of GAM, thus, requires $\omega_0^2 > \omega_A^2/4$, i.e., the pump TAE lies in the upper half of the toroidicity induced gap, which is not the general case. The threshold condition for the parametric instability can be estimated as $(\delta B_r/B_0) \sim O(10^{-4})$, comparable with other mode-mode coupling channels [153, 161–163]. Note that, as it was pointed out in [156], ZS excited by weakly ballooning Alfvén eigenmodes may have a fine scale radial structure in addition to the well-known meso-scale radial envelope considered here, which may further enhance the nonlinear coupling, leading to faster GAM excitation and lower threshold.

4.3. Nonlinear GAM excitation by DWs: global theory

4.3.1. Finite DW/GAM dispersiveness: convective amplification and nonlinear GAM group velocity. When finite interaction region due to finite pump DW radial envelope is taken into account, effects of finite GAM and DW sideband group velocities play important roles in the nonlinear dynamics [46]. Neglecting system nonuniformities due to ω_* and GAM continuum while retaining finite pump DW radial envelope, i.e., considering a time scale shorter than L_P/V_c with V_c defined later, equations (45) and (46) become

$$(\partial_\tau + V_S\partial_\xi)A_S = \Gamma_0^*(\xi)\mathscr{E}_G, \tag{57}$$

$$(\partial_\tau + V_G\partial_\xi)\mathscr{E}_G = \Gamma_0(\xi)(k_r^2 - 2\mathrm{i}k_r\partial_\xi)A_S. \tag{58}$$

In deriving the above equations, two temporal and spatial scale expansion, $\partial_t = -\mathrm{i}\omega + \partial_\tau$ and $\partial_r = \mathrm{i}k_r + \partial_\xi$, are applied. Here, $V_S = C_d\omega_{*0}\rho_{ti}^2k_r$ and $V_G = G\omega_G^2(0)\rho_{ti}^2k_r/(2\omega)$ are respectively, the linear group velocities of DW sideband and GAM. Note that finite dissipation due to γ_S and γ_G are neglected, as we focus on the global properties of the parametric instability [131

The parametric instability with both daughter waves having a linear group velocity is discussed in [131]. As main result, the instability is a convective amplification process when the two daughter waves propagate in the same direction (equivalent to $C_dG > 0$ for the case considered here); while absolute instability exists if the two daughter waves propagate in opposite directions (i.e., $C_dG < 0$). Equations (57) and (58) are solved numerically, with fixed $C_d = 1$ and changing the sign of G to explore both cases. The results are shown in figure 14. It is clearly seen that, for $GC_d > 0$ (DW sideband and GAM propagate in the same direction), the parametric instability is a convective amplification process; while for $C_dC_G < 0$ it is an absolute instability. Due to the finite pump DW radial width, for $C_dG > 0$, the coupled DW sideband and GAM wave packet may propagate out of the unstable region of the parametric instability before they are well developed. The value of C_d is typically positive, while the sign of G is investigated carefully in [12]. For typical tokamak parameter, we have $G > 0$. As a result, the nonlinear excitation of GAM, is typically a convective instability within the present analysis.

The radial propagation of GAM has been observed in experiments [21, 129, 164–166], investigated in numerical simulations [31, 120, 167], and computed analytically based on linear KGAM dispersion relation [12] considering short wavelength structure generation due to the GAM continuous spectrum [38, 40, 41]. However, when the experimental data [21] and numerical results [120] are compared with KGAM dispersion relation, the obtained coefficient for kinetic dispersiveness is much bigger than that predicted by linear theory and due to FLR and FOW of ions. The nonlinear velocity of the coupled DW sideband and GAM wave packets discussed above, provide another interpretation; noting that in experiment [21], the GAM is driven by ambient turbulence.

Moving into the wave frame by taking $\zeta = \xi - V_ct$ with $V_c = (V_S + V_G)/2$, and taking $\mathscr{E}_G = \exp(\mathrm{i}\hat{\beta}\zeta)\hat{A}(\zeta, \tau)$ with $\hat{\beta} \equiv k_r\Gamma_0^2/(2V_0^2)$ and $V_0 \equiv (V_S - V_G)/2$, the coupled nonlinear equations (57) and (58) can be combined into

$$(\partial_\tau^2 - V_0^2\partial_\zeta^2)\hat{A} = (k_r^2\Gamma_0^2 - \mathrm{i}k_r\Gamma_0^2\partial_\zeta)\hat{A} \equiv \hat{\eta}^2\hat{A}, \tag{59}$$

which can be solved and yields the following unstable solution:

$$\hat{A} = \frac{\hat{A}_0}{\sqrt{\pi}\Delta k_0}\int_{-\infty}^{\infty}\mathrm{d}k_I \times \exp\left[-\frac{k_I^2}{\Delta k_0^2} + \mathrm{i}k_I\zeta + \sqrt{\hat{\eta}^2 - k_I^2V_0^2}\,\tau\right]. \tag{60}$$

This is the solution for a typical initial condition $\hat{A} = \hat{A}_0\exp(-\Delta k_0^2\zeta^2/4)$ at $\tau = 0$; i.e., the parametrically excited GAM has a finite initial spectrum width Δk_0. As the convective damping due to dispersiveness is smaller compared to the temporal growth, i.e., $|V_c\partial_\zeta| \ll |\partial_\tau|$, the time asymptotic

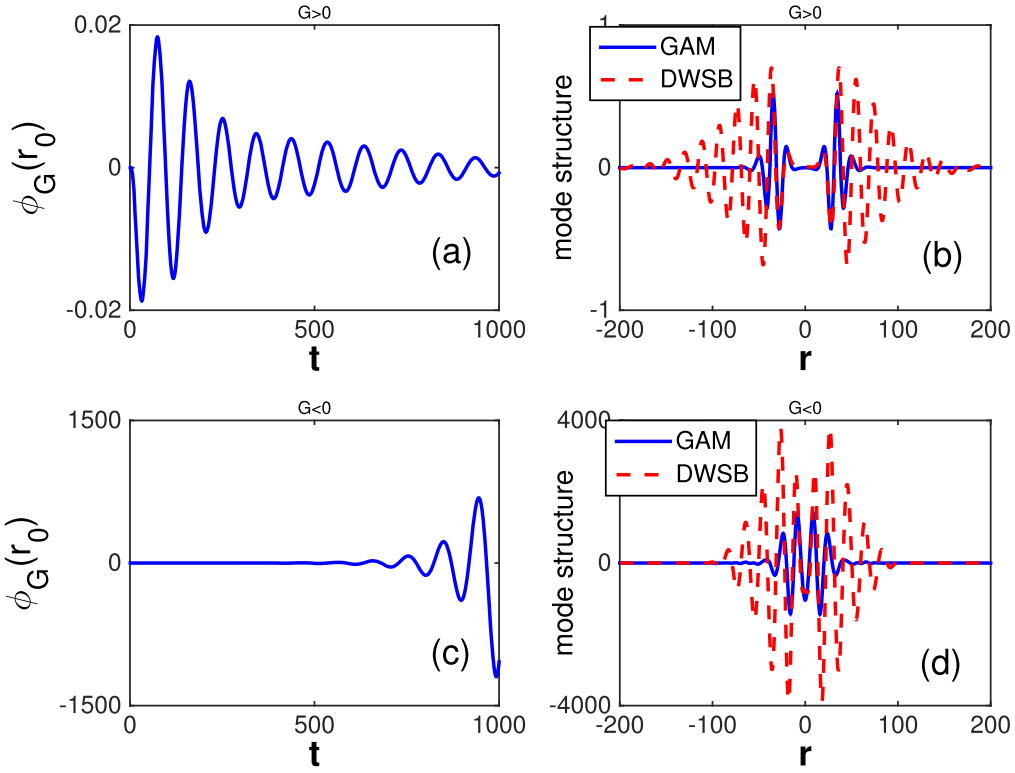

Figure 14. (Reproduced from figure 1 of [46].) (a) and (c) are respectively the GAM amplitude at r_0 versus time for $G = \pm 1$. (b) and (d) are respectively the snapshot of mode structure at $t = 100/\omega_G$ for $G = \pm 1$.

solution of GAM electric field is then

$$\mathscr{E}_G = \frac{\hat{A}_0}{\Delta k_0 \lambda_\tau} \exp\left[\hat{\eta}\tau + \mathrm{i}\hat{\beta}(\zeta - V_c\tau) - \frac{(\zeta - V_c\tau)^2}{4\lambda_\tau^2}\right]. \quad (61)$$

From the second term in the exponent, it is clear that $\hat{\beta}$ can be interpreted as the nonlinear modification of the GAM wave vector, while it also affects the GAM frequency through $\hat{\eta}$. $\lambda_\tau \equiv \sqrt{1/\Delta k_0^2 + V_0^2\tau/(2\hat{\eta})}$ describes the broadening of the initial GAM pulse during the propagation.

The solution in equation (61) provides direct information for the interpretation of experimental observations [21, 168] and/or nonlinear simulations [120]. The parametrically excited GAM is characterized by a nonlinear radial wavenumber

$$k_{\mathrm{NL}} = k_r - \mathrm{i}\partial_\zeta \ln \mathscr{E} = k_0(1 + \Gamma_0^2/(2V_0^2)), \quad (62)$$

and a nonlinear frequency

$$\omega_{\mathrm{NL}} = \omega_0 + \mathrm{i}\partial_\tau \ln \mathscr{E} = \omega_0 + \frac{k_0\Gamma_0^2 V_c}{2V_0^2}. \quad (63)$$

Both increase with the pump DW amplitude. The frequency and wavenumber at vanishing Γ_0, (ω_0, k_0), can be solved from the matching conditions, which can be substituted into equation (63) and yields,

$$\omega_{\mathrm{NL}} = \omega_G + \frac{k_0\Gamma_0^2 V_c}{2V_0^2} + \frac{G\omega_G\rho_{ti}^2 k_{\mathrm{NL}}^2}{4(1 + \Gamma_0^2/(2V_0^2))^2}. \quad (64)$$

Note that, V_c and V_0 are both proportional to k_0, and, thus, the frequency increment due to finite amplitude pump DW, $k_0\Gamma_0^2 V_c/(2V_0^2)$, is independent of k_0. The frequency increment, can be expressed as $(e\delta\phi/T)^2(L_n/\rho_{ti})^2$ from our theory, which indicates an order of unity frequency increment for typical parameters. This may explain the existence of the higher frequency branch of the 'dual-GAM' observed in HT-7 tokamak [21], which has a frequency almost double of the local GAM frequency.

The obtained expressions of the frequency and wavenumber of the parametrically excited GAM, equations (63) and (62), are compared with the numerical solutions of equations (57) and (58) shown in figures 15 and 16, respectively, and the analytical solutions fit well with the numerical results.

The nonlinear dispersion relation of the parametrically excited GAM, $\omega_{\mathrm{NL}}(k_{\mathrm{NL}})$, is plotted in figure 17; along with the linear dispersion relation $\omega_0(k_0)$. Note that, the vertical and horizontal axes are, respectively, the 'observed' frequency and wavenumber. The frequency increment due to finite amplitude pump DW has a weak dependence on the wavenumber. Thus, the 'effective' G obtained from experiments [21] or simulations [120] should be smaller than that derived from linear KGAM theory [39]. However, if only one point is obtained from experiments/simulations and then fitted with the linear dispersion relation [39], overestimation of 'G' will be made, as shown by the dashed line. From a rough estimation using typical parameters, the misinterpretation may lead to an $O(10^2)$ overestimation of the 'G', consistent with that reported in literatures [21, 120].

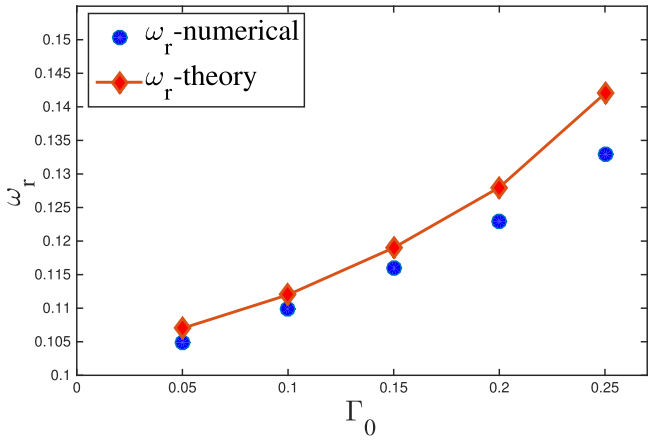

Figure 15. (Reproduced from figure 3 of [169].) Dependence of parametrically excited GAM frequency on pump DW amplitude.

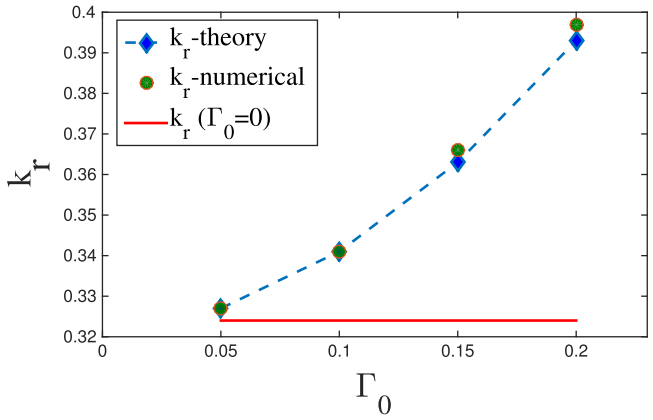

Figure 16. (Reproduced from figure 1 of [169].) Dependence of parametrically excited GAM wavenumber on pump DW amplitude.

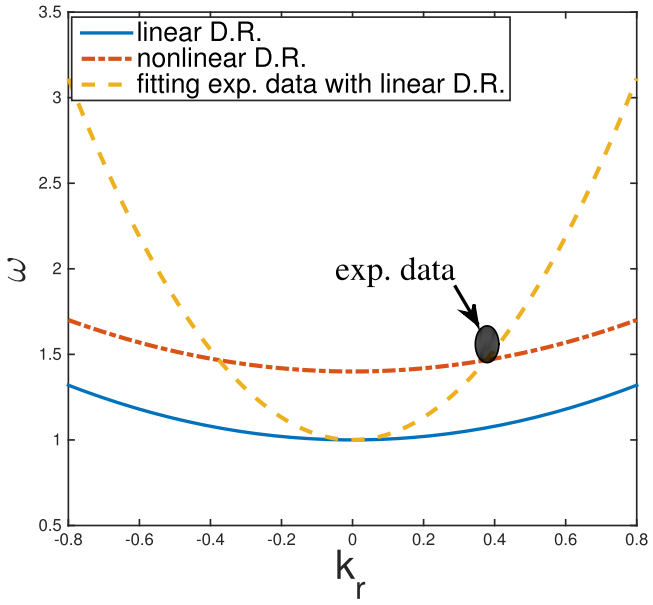

Figure 17. Nonlinear dispersion relation of parametrically excited GAM.

4.3.2. Non-uniform plasma: quasi-exponentially growing absolute instability. Note that, in the above analysis, we have neglected plasma nonuniformity and, thus, the analisis is valid for a time scale shorter than L_P/V_c. Next, we consider the longer time scale, and take the nonuniformity of $\omega_*(r)$ into account, while we neglect the contribution of GAM continuum in order to illustrate the effects of non-uniform $\omega_*(r)$. Equations (45) and (46) are solved numerically, and the result shows that outward propagating coupled DW sideband and GAM wave packets are reflected at the DW turning points due to $\omega_*(r)$ nonuniformity, and are amplified as they propagate through their original position r_0 again. The convective instability, as a result, becomes a quasi-exponentially growing absolute instability.

In the strong drive limit with $|\omega^2 - \omega_G^2| \simeq |2\gamma\omega_G| \gg |G\omega_G^2\rho_i^2k_r^2/2|$, the KGAM kinetic dispersiveness term can be ignored, and the coupled equations can be combined to yield the nonlinear DW sideband eigenmode equation in Fourier-k_r space [44, 170]

$$\left(\frac{\omega_*}{L_*^2}\frac{\partial^2}{\partial k_r^2} + \omega - \omega_P + \omega_* - C_d\omega_*\rho_{ti}^2k_r^2 + \frac{\omega k_r^2\Gamma_0^2}{\omega^2 - \omega_G^2}\right)A_S = 0. \tag{65}$$

The linear DW eigenmode equation can be recovered if one ignores the nonlinear term (the term proportional to Γ_0^2) in equation (65), and it can be solved to yield the finite extent of the pump DW in k_r space, and, equivalently, the localization in real space with a typical scale length $\propto\sqrt{L_*\rho_{ti}}$. Including the nonlinear term, equation (65) yields the following nonlinear dispersion relation

$$\frac{L_*^2}{\omega_*}(\omega - \omega_P + \omega_*)\tilde{\beta}^2 = 2l + 1, \quad l = 0, 1, 2, 3 \ldots \tag{66}$$

with $\tilde{\beta}$ given by

$$\tilde{\beta}^4\frac{L_*^2}{\omega_*}\left(C_d\omega_*\rho_i^2 + \frac{\omega\Gamma_0^2}{\omega_G^2 - \omega^2}\right) = 1.$$

The eigenmode structure of DW sideband in Fourier space is given by

$$A_S \propto \exp\left(-\frac{k_r^2}{2\tilde{\beta}^2}\right), \tag{67}$$

with a radial extent of $|\tilde{\beta}|^{-1}$ [21, 164, 171, 172]. This explains the localization of GAM by 'density pedestal' reported in [172], where GAM can only be observed in the density gradient region where density gradient is sharp (i.e., L_* small compared to the plasma minor radius); whereas GAM can be observed well into the plasma when the pedestal weakens.

Finally, with all the nonuniformities self-consistently included, the coupled nonlinear equations (45) and (46), are solved numerically. The time histories of GAM amplitude at $r = r_0$ is shown in figure 18, in which the solid curve

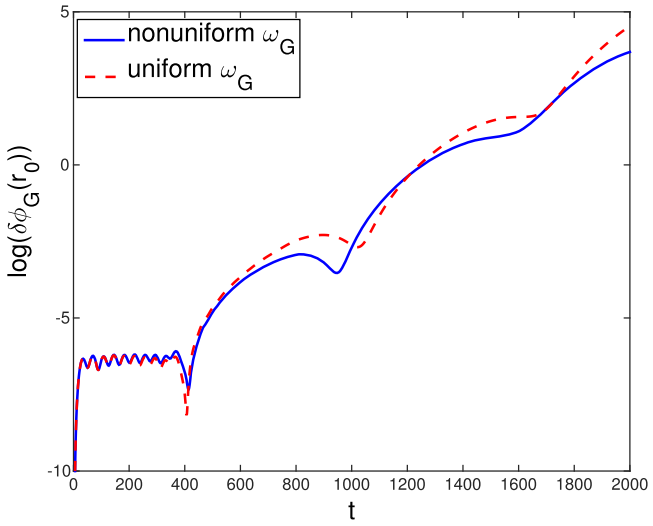

Figure 18. (Reproduced from figure 6 of [46].) Mode structures at $t = 500$.

corresponds to the non-uniform GAM frequency case, while the dashed line illustrates the uniform GAM frequency case for comparison. One notes that the two cases are qualitatively similar, i.e., the nonuniformity of $\omega_*(r)$ is the dominant effect on the longer time scale, which renders the initially convective parametric instability into a quasi-exponentially growing absolute instability on a longer time scale. On the other hand, GAM continuum plays a relatively minor role. Due to the frequency mismatch induced by spatially varying $\omega_G(r)$, the case with non-uniform $\omega_G(r)$ has a slightly different growth rate. The mode structures of coupled DW sideband and GAM at six different times are shown in figure 19. One may see that, due to the nonuniformity induced by GAM continuum, the mode structures propagating in opposite directions are not symmetric. The wave packet initially propagating outward has a larger k_r and, thus, larger growth rate and group velocity. Consequently, one may observe that it also has a larger amplitude; then, it is reflected at the turning point induced by ω_* nonuniformity, and propagates inward, completing a full 'bouncing' period of wave packets radially trapped by non-uniform ω_*.

Note that, although extensively studied in the past two decades, most publications on the nonlinear interactions of GAM and DW turbulence focuses on the 'linear growth stage' of the parametric instability, i.e., considering a fixed amplitude DW decays into a GAM and a DW sideband, while the feedbacks of DW sideband and GAM on the pump DW are neglected. As a result, the theories cannot be applied to the nonlinear dynamics of DWs mediated by GAMs, e.g., at saturation. An attempt is made in [12], where the feedbacks of the DW sideband and GAM to the linearly unstable DW pump are considered. The derived driven-dissipative system based on three-wave couplings then exhibits limit-cycle behaviors, period-doubling and route to chaos as possible indication of the existence of strange attractors [132], which can be applied to interpret experimental observations such as 'predator-prey' behaviors of GAM and DW intensity. However, in the truly nonlinear stage, the strongly modulated DW can no longer be separated as a pump and a sideband. The two field model for DW-GAM system, described by equations (41) and (42), including full radial wavenumber spectrum should be used, as in the nonlinear dynamics of the coupled DW-ZFZF system [134].

5. Nonlinear self-coupling of GAM/EGAM

Nonlinear self-couplings of GAMs were observed in experiments [33, 73, 173], in the form of perturbations at GAM second harmonic frequency, and considered to be important for DW nonlinear dynamics as an additional channel for saturating GAMs [34]. In GTC [110] simulations with a finite amplitude GAM as initial condition, scalar potential generation at GAM second harmonic frequency was observed in the absence of parallel nonlinearity. However, GAM second harmonic generation was suppressed when parallel nonlinearity was turned on. Analytical theory based on phase space volume conserving gyrokinetic equation [53, 54, 174] explained these simulation results with the exact cancellation of parallel and perpendicular nonlinearity to the leading order [34]. No GAM second harmonic scalar potential generation is also obtained from fluid theory, with emphasis on the associated second harmonic density perturbation [35].

Even if not emphasized explicitly, the simulations in [34] also show finite ZFZF scalar potential generation by GAM. This process is not affected by the cancellation of parallel and perpendicular nonlinearities. The analysis based on gyrokinetic theory [37] shows that finite ZFZF generation is due to thermal ion FOW effects, so it is a purely 'neoclassical' effect with contribution from toroidal geometry. It is also shown that there is no modulation of GAM by ZFZF.

The GAM second harmonic and ZFZF generation discussed above may have direct impact on the nonlinear dynamics of DW turbulences discussed in section 4, because of the effect of ZFZF on regulating DWs [5, 26, 109, 110, 132, 136, 137]. Generation of GAM second harmonic, which is not a normal mode of the system, will induce additional dissipation for GAMs. Meanwhile, ZFZF generation by GAM corresponds to direct power transfer from GAM to ZFZS. Both processes will affect the branching ratio of GAM and ZFZF generation by DWs, and, thus, the nonlinear dynamics of DWs.

To understand the GAM second harmonic scalar potential generation, it is shown in [35] that the contribution from resonant EPs will induce EGAM second harmonic scalar potential. Therein, a perturbative model in the small EP drift orbit limit is analyzed for the simplicity of discussion. The general theory of second harmonic and ZFZF generation by EGAM is given in [36], which can be applied for arbitrary wavelengths.

In the following, the analysis of [34] will be briefly reviewed, with emphasis on the conditions for the cancelation of parallel and perpendicular nonlinearities. The other self coupling channels, investigated in [35–37], will be discussed based on the result of [34].

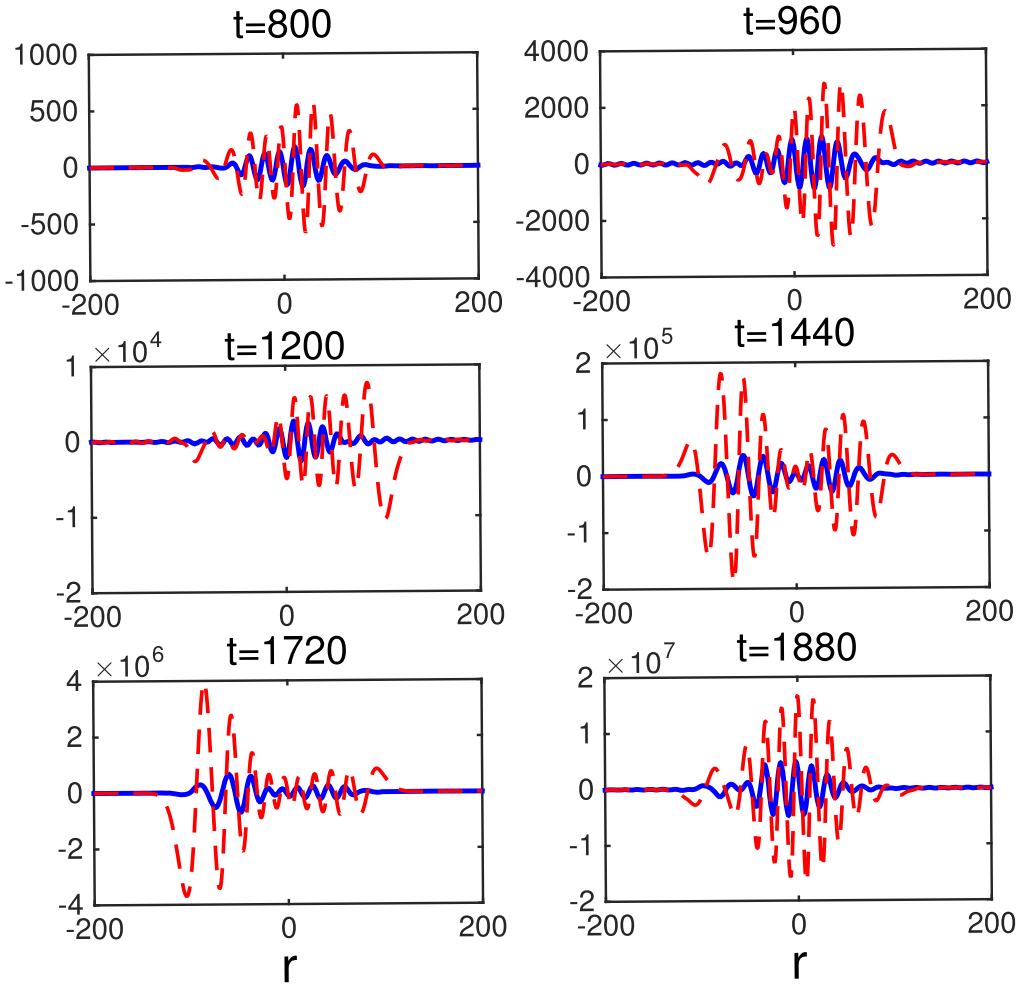

Figure 19. (Reproduced from figure 5 of [46].) Snapshots of mode structure at different times.

5.1. GAM second harmonic generation

For GAM second harmonic generation by self beating of GAM with $k_\parallel = 0$, the nonlinear gyrokinetic equation in the phase-space volume conserving form [53, 54] can be written as:

$$(\partial_t + v_\parallel \partial_l + \mathrm{i}\omega_d)\delta F_{\mathrm{II}} = -\hat{\mathbf{b}} \times \nabla J_G \delta\phi_G \cdot \nabla \delta F_G / B - \delta\dot{v}_\parallel \partial_{v_\parallel} \delta F_G, \tag{68}$$

with the first term on the rhs being the usual perpendicular convective nonlinearity, and the second term being the parallel nonlinearity, which is usually neglected in the gyrokinetic equation (10). In fact, the latter is typically of higher order when compared with the perpendicular nonlinearity. Here, $\delta\dot{v}_\parallel \equiv -e\hat{b} \cdot \nabla J_G \delta\phi_G / m - \nabla \times (v_\parallel \hat{\mathbf{b}}) \cdot \nabla J_G \delta\phi_G / B$, and the subscript 'II' is used for second harmonic. The GAM second harmonic dispersion relation can be obtained from quasi-neutrality condition, and one has

$$-\frac{e}{m} n_0 k_{\mathrm{II}}^2 \frac{1}{\Omega_i^2} \left(1 - \frac{\omega_G^2}{\omega_{\mathrm{II}}^2}\right) \overline{\delta\phi}_{\mathrm{II}} + \langle \overline{\delta F_{\mathrm{II}}} \rangle = 0, \tag{69}$$

with the second harmonic perturbation derived as

$$\delta F_{\mathrm{II}} = -\frac{k_G \overline{\delta\phi}_G \hat{F}}{\omega_{\mathrm{II}} B_0} \left[\frac{\cos\theta}{r(1 - \epsilon\cos\theta)} - \frac{\sin^2\theta}{R_0} \right]. \tag{70}$$

Here, $\hat{F} \equiv \delta F_G / \sin\theta \simeq (e/T_i)(\hat{\omega}_{dr}/\omega) F_0 J_G \overline{\delta\phi}_G$, and the two terms in equation (70) are respectively, the perpendicular and parallel nonlinearity contribution. The perpendicular nonlinearity is formally $O(\epsilon^{-1})$ larger, as expected, giving the dominant 'up–down symmetric' ($\propto\cos\theta$) second harmonic density perturbation [33–35]. However, since the GAM second harmonic dispersion relation is derived from the surface averaged quasi-neutrality condition, the dominant perpendicular nonlinearity proportional to $\cos\theta$, can only have a contribution via the toroidicity term in its denominator, as explicitly given in equation (70). As a result, the contribution from parallel and perpendicular nonlinearity cancels exactly upon taking the flux surface average. Thus, there is no GAM second harmonic scalar potential generation up to the order of parallel nonlinearity.

Note that, in the case discussed here, the perpendicular nonlinearity, which is larger by $O(\epsilon^{-1})$, contributes to scalar potential generation through toroidal coupling, making the contribution $O(\epsilon)$ smaller, and cancels exactly with parallel

nonlinearity. Other processes are then required to have a non-vanishing density perturbation, after surface averaging, producing finite self coupling of GAMs and generation of GAM second harmonic and/or ZFZF on a time scale shorter than the parallel nonlinearity characteristic time. There are two mechanisms that have been suggested in the literature as possible candidates. One is the coupling through thermal ion FOW effects, proposed in [37] for $k_r\rho_{d,i} > \epsilon$; and another one is via EP FOW effects, which are of larger EP drift orbits but the tradeoff of smaller EP concentration [35, 36]. For the sake of completeness, we also note that the symmetry breaking induced by finite amplitude DWs in GAM second harmonic and ZFZF generation has been investigated in the literature [175, 176], and is related to the long time scale evolution of the coupled DW-GAM system [74, 134, 135]. A detailed discussion of these processes is beyond the scope of the present brief review.

5.2. ZFZF generation by GAM

ZFZF generation is observed in the above mentioned GTC simulations, with or without inclusion of parallel nonlinearity [34]. This suggests that other mechanisms, stronger than toroidal coupling discussed in section 5.1, may be responsible for the ZFZF generation. Motivated by this evidence, it was shown [37] that thermal ion FOW effects may generate ZFZF scalar potential for $k_G\rho_{d,ti} > \epsilon$, with the contribution from perpendicular nonlinearity being significantly larger than parallel nonlinearity after surface averaging. The nonlinear gyrokinetic equation for ZFZF generation by self beating of GAM, can be written as

$$(\partial_t + v_\parallel\partial_l)\delta H^{\rm NL}_{dZ} = -{\rm e}^{-{\rm i}k_Z\rho_d}\frac{1}{B}\hat{\mathbf{b}}\times\nabla\delta\phi_G\cdot\nabla\delta H_G, \quad (71)$$

with $\delta H^{\rm NL}_{dZ} = {\rm e}^{{\rm i}k_Z\rho_d}\delta H^{\rm NL}_Z$ being the drift orbit center distribution function, ${\rm e}^{{\rm i}k_Z\rho_d}$ representing the operator for drift orbit center transformation and $\rho_d = \hat{v}_d\cos\theta/\omega_{tr} \equiv \hat{\rho}_d\cos\theta$ being the drift orbit width defined below equation (13).

For ZFZF, with $\omega_Z \ll |v_\parallel\partial_l|$, one has $\delta H^{\rm NL}_{dZ} = \overline{\delta H^{\rm NL}_{dZ}} + \widetilde{\delta H^{\rm NL}_{dZ}} \simeq \overline{\delta H^{\rm NL}_{dZ}}$. Therefore,

$$\partial_t\overline{\delta H^{\rm NL}_{dZ}} = -\frac{c}{B_0}\overline{{\rm e}^{-{\rm i}k_Z\rho_d}\sum_{\mathbf{k}}\hat{\mathbf{b}}\times\nabla\delta\phi_G\cdot\nabla\delta H_G}. \quad (72)$$

Noting that $\delta\phi_G = \overline{\delta\phi}_G + \delta\phi_{G,1}\sin\theta$, $\rho_d \propto \cos\theta$, $\omega_d \propto \sin\theta$, assuming $|k_Z\rho_d| \ll 1$, using the expression of δH_G derived in section 2.2 and noting $\omega_G = \omega_0 + {\rm i}\partial_t$, we then have, after some algebra [37]

$$\overline{\delta H^{\rm NL}_{dZ}} = -\frac{e}{T_i}F_0\frac{1}{\omega_0^2}\frac{c}{B_0}\hat{v}_d\overline{\rho_d\cos\theta}\frac{\partial}{\partial r}\left(\frac{|\delta E_{G,r}|^2}{r}\right). \quad (73)$$

It is worth mentioning that the dominant contribution comes from coupling due to finite drift-orbit width effect; that is, a neoclassical effect. Substituting the nonlinear particle response, equation (73), into the quasi-neutrality condition, we obtain the following nonlinear equation describing nonlinear excitation of ZFZF by a finite amplitude GAM

$$\chi_Z\overline{\delta\phi_Z} = -\frac{c}{B_0}\frac{1}{\omega_G^2}\frac{\partial}{\partial r}\left[\langle\hat{v}_d\overline{\cos\theta\rho_d}F_0\rangle\frac{|\overline{\delta E_G}|^2}{r}\right]; \quad (74)$$

where, χ_Z is the well-known neoclassical polarization [2]

$$\chi_Z\overline{\delta\phi_Z} \equiv \left(1 - \left\langle\frac{F_0}{n_i}J_Z^2\,|\overline{{\rm e}^{{\rm i}k_Z\rho_d}}|^2\right\rangle\right)\overline{\delta\phi_Z}.$$

On the other hand, there is no modulation of GAM by ZFZF up to the order of parallel nonlinearity, which is beyond the time scale of interest. Thus, the nonlinear generation of ZFZF by GAM observed in [34] is a forced driven process, which is, again, underlying the $\omega_G = \omega_{Gr} + {\rm i}\partial_t$ condition used for deriving the non-vanishing ion response of ZFZF in equation (73).

5.3. Second harmonic generation by EGAM

To understand the finite GAM second harmonic scalar potential generation, the effect of EPs was proposed and analyzed in [35], where resonant EP contribution was treated in the small EP drift orbit limit. The analysis is then extended to arbitrary wavelengths in [36], for the GAM second harmonic and ZFZF generation. The basic ideas of [35, 36] are consistent with those of [37], i.e., taking the coupling due to EP FOW into account (noting again $\rho_{d,h} \propto \cos\theta$). In particular, EPs are characterized by larger drift orbits than thermal ions [37]; however, EPs have much smaller density.

Here, we will briefly review the approach of [36] using the same gyrokinetic theoretical framework consistent with the rest of the current review, although the original analysis is proposed in [35] for the EGAM second harmonic generation. Generation of ZFZF by EGAM is also investigated in [36] and can be derived following the same approach. Again, only processes faster than parallel nonlinearity are of interest here. Substituting the EP response from equation (13) into equation for nonlinear EP drift orbit center distribution function, and considering small but finite T_e/T_i, we then obtain the following general expression of the nonlinear EP response to the EGAM second harmonic

$$\begin{aligned}\delta H^{\rm NL}_{{\rm II},h} = {\rm i}k_r\frac{c}{B_0}\partial_E F_{0,h}\sum_{\eta,\xi,p,l}&\frac{p+l}{\omega_{\rm II} - (p+\xi+l)\omega_{tr}}\\ &\times i^{\eta+p-\xi-l}{\rm e}^{{\rm i}(\eta+p+\xi+l)\theta}J_\eta(\hat{\Lambda}_{{\rm II},h})J_\xi(\hat{\Lambda}_{{\rm II},h})\\ &\times J_l(\hat{\Lambda}_h)J_p(\hat{\Lambda}_h)\frac{\omega}{\omega - l\omega_{tr}}\frac{\overline{\delta\phi}_G\overline{\delta\phi}_G}{r}.\end{aligned} \quad (75)$$

Here, $\hat{\Lambda}_h = k_r\hat{\rho}_{d,h}$ and $\hat{\Lambda}_{II,h} = k_{r,II}\hat{\rho}_{d,h} = 2\hat{\Lambda}_h$. Substituting equation (75) into the surface averaged quasi-neutrality condition, we obtain the equation for EGAM second harmonic generation:

$$\hat{b}_{\rm II}\mathscr{E}_{\rm EGAM}(\omega_{\rm II})\frac{en_0}{T_i}\overline{\delta\phi}_{\rm II} = -\langle\overline{\delta H^{\rm NL}_{{\rm II},h}}\rangle, \quad (76)$$

where $\hat{b}_{\rm II} \equiv k^2_{r,{\rm II}}\rho^2_{L,h}/2$, and $\mathscr{E}_{\rm EGAM}(\omega_{\rm II})$ is the linear EGAM dielectric function at $\omega = \omega_{\rm II}$, with nonadiabatic EP response given by equation (13). The general dispersion relation obtained from equation (76) will recover that of [35] in the

proper limit, i.e., with $|\Lambda_h| \ll 1$ and only resonant EP contributions taken into account.

For EGAM with a typically global mode structure, i.e., $|\Lambda_h| \ll 1$, the dominant contribution is obtained for small $|\eta| + |\xi| + |p| + |l|$. Also, $l = \pm 1$ can be assumed the strongest linear EGAM drive, and $p + l \neq 0$ is required for non-vanishing nonlinear EP response to EGAM second harmonic. With these selection rules in mind, and noting that $\omega_{\rm II} = 2\omega$ and $\hat{\Lambda}_{{\rm II},h} = 2\hat{\Lambda}_h$, one then has

$$\overline{\delta H^{\rm NL}_{{\rm II},h}} \simeq {\rm i}\frac{c}{B_0}\frac{\partial F_{0,h}}{\partial E}\frac{3k_r\omega\hat{\omega}^2_{dr}}{(\omega^2-\omega^2_{tr})(\omega^2_{\rm II}-\omega^2_{tr})}\frac{\overline{\delta\phi}_G\overline{\delta\phi}_G}{r}. \quad (77)$$

We note that equation (77) is equivalent to equation (51) of [35]. Substituting equation (77) into the quasi-neutrality condition for EGAM second harmonic, we then obtain:

$$\hat{b}_{\rm II}\mathscr{E}_{\rm EGAM}(\omega_{\rm II})\overline{\delta\phi}_{\rm II} = -\frac{{\rm i}k_r T_i}{n_0 m\Omega_i r}\left\langle\frac{3\omega\hat{\omega}^2_{dr}\partial_E F_{0,h}}{(\omega^2-\omega^2_{tr})(\omega^2_{\rm II}-\omega^2_{tr})}\right\rangle\overline{\delta\phi}^2_G, \quad (78)$$

with $\mathscr{E}_{\rm EGAM}(\omega_{\rm II})$ obtained from the proper limit of the linear EGAM second harmonic dispersion relation for small magnetic drift orbits and only primary transit resonance accounted for in the nonadiabatic EP response. Note that, in equation (52) of [35], $\omega_{\rm EGAM}$ should also be a function of $\omega_{\rm II}$ (ω_2 using the notation of [35]). Equation (78) or, more precisely, equation (76) can then be applied to explain experimental observations/simulation results on EGAM second harmonic generation, by directly substituting parameters into the nonlinear dispersion relation along with both the amplitude and radial mode structure of the primary mode.

6. Unified theoretical framework of GAM/EGAM

The physics processes discussed above can be synthetically included into the following 'unified theoretical framework' of GAM/EGAM [74]; including self-consistent generation of GAM by DW turbulences and/or EPs, modulation of DW by GAM/EGAM, and self-consistent evolution of EP equilibrium distribution function due to nonlinear interactions with GAMs. The corresponding equations are

$$\omega_d D_d A_d = \frac{c}{B_0}\frac{T_i}{T_e}k_\theta A_d\partial_r A_G, \quad (79)$$

$$\omega_G\mathscr{E}_{\rm EGAM}\partial_r A_G = -\frac{\alpha_i c}{B_0}k_\theta(A_d\partial^2_r A^*_d - {\rm c.c.}). \quad (80)$$

Here, $\mathscr{E}_{\rm EGAM}$ is the EGAM dispersion relation obtained from equation (17)

$$\mathscr{E}_{\rm EGAM} \equiv -1 + \frac{\omega^2_G(r)}{\omega^2} - \frac{G}{2}\rho^2_{ti}\partial^2_r + \frac{\overline{\delta n}_h m_i\Omega^2_i}{en_0 k_r^2\overline{\delta\phi}_G},$$

with the perturbed EP density δn_h give by equation (18), where the slowly varying EP 'equilibrium' distribution function $F_{0,h}$ due to emission and reabsorption of EGAM is the solution of the Dyson equation (38). Thus, this 'unified theoretical framework', based on equations (38), (79) and (80), fully describes GAM related physics in realistic geometries; including linear physics of GAM/EGAM, nonlinear dynamics of EGAM and nonlinear dynamics of the coupled GAM/EGAM-DW system. Note that EP interaction with DWs is typically weak [60, 61]. We incidentally note that the $\mathscr{E}_{\rm EGAM}$ expression defined here [43], besides the EP contribution in δn_h, has a coefficient $k_r^2\rho^2_{ti}/2$ compared to $\mathscr{E}_{\rm GAM}$ [46, 119, 138] used in section 4 due to the different notations used in original papers. Note also that equations (79) and (80) are derived based on $k_\perp\rho_{ti} \ll 1$ expansion; while no separations of DW into pump and sidebands is assumed. As a result, neglecting EP effects, the DW-GAM system described by the two field model, equations (79) and (80), can be applied to understand the fully nonlinear evolution of DWs, including turbulence spreading and saturation due to the envelope modulation by GAMs [134]. Meanwhile, when A_d is separated into a fixed amplitude pump DW and its sideband due to GAM modulation (distortion of parallel mode structure is not significant in nonlinear processes with $\tau_{\rm NL} \gg \omega^{-1}$), equations (45) and (46) are recovered, as shown in [74].

Linear excitation and nonlinear evolution of EGAM, on the other hand, can be described by equations (38) and (80) in the absence of DWs. If, for example, the equilibrium EP distribution function is used, equation (80) then describes the linear EGAM excitation, as discussed in sections 3.1 and 3.2. When the slow EP distribution function evolution on transport time scale due to emission and re-absorption of EGAM is taken into account, equations (38) and (80) could then provide the self-consistent EGAM nonlinear dynamics qualitatively discussed in section 3.3. Thus, the 'unified theoretical framework of GAM/EGAM' includes all the physics presented in this review. It also provides the outlooks for possible future research on the dynamics evolution of the fully nonlinear system.

7. Conclusions and discussions

In this paper, the recent theoretical understandings of GAMs are briefly reviewed; including the linear dispersion properties, resonant excitation by EPs, nonlinear excitation by DWs/DAWs, and the nonlinear self-coupling of GAM/EGAM. The emphasis is on the effects of system nonuniformities, the requirements of first-principle-based kinetic treatments, and global theory. We emphasized that, although quite broad topics related to GAMs are investigated in the past two decades, the interest of the fusion community on GAMs is due to their potential capabilities of regulating microscale turbulences and the associated anomalous transport. Consequently, the research on GAMs is carried out aiming toward the final goal of understanding the nonlinear dynamics of DWs and transport in the presence of GAMs.

In section 2, an important concept of GAM is introduced, i.e., GAM continuous spectrum due to system nonuniformity, which leads to the generation of short scale mode structures and the breakdown of fluid description. As a result, kinetic treatment is required for the dispersion relation of short wavelength KGAM; e.g., the Landau damping rate due to

wave–particle resonance at short wavelength, and the accurate prediction of the kinetic dispersiveness due to FLR and FOW effects; both playing important roles in the nonlinear interactions with DWs, as noted in section 4.

In section 3, the resonant excitation and nonlinear saturation of EGAM are reviewed, using the analogy to the well-known BPI. One crucial difference of the EGAM in three dimensional torus with respect to BPI in a strongly magnetized plasma is the EGAM radial mode structure due to the coupling to GAM continuous spectrum; leading to global mode structure and finite threshold condition. Nonlinear interactions of EGAM and DWs are observed in numerical simulations, and thus, EGAM is considered as a potential active control for DW turbulences. The Dyson equation describing nonlinear saturation of EGAM due to wave–particle phase space nonlinearities is also derived, and qualitative discussions of the phase space structure generation and secular nonlinear EGAM dynamics are made.

In section 4, the nonlinear excitation of GAM by DWs/DAWs is investigated, and it is shown by local theory that short wavelength KGAM is preferentially excited. The theory based on $k_\perp \rho_{ti} \ll 1$ expansion, valid for GAM excitation by ITG DW, is then extended to $k_\perp \rho_{ti} \sim O(1)$ to discuss the excitation by CTEMs and by TAEs, where electro-magnetic nonlinearity associated with Maxwell stress is also considered. The global theory including kinetic dispersiveness of both DW and KGAM and finite pump DW radial scales shows that the parametric instability, which is a convective amplification process on the short time scale, becomes a quasi-exponentially growing absolute instability on the longer time scale, when nonuniformity of DW drive, i.e., diamagnetic drift frequency, is taken into account. The qualitative change of the parametric process further shows the importance of kinetic treatment and system nonuniformity in proper analysis of the DW nonlinear dynamics and the resultant transport level.

In section 5, the nonlinear self-couplings of GAM/EGAMs are investigated; with GAM second harmonic generation as an additional channel for GAM dissipation, and ZFZF generation as a channel for power transfer from GAM/EGAM to ZFZF. An important control parameter for the nonlinear process is $k_r \rho_d/\epsilon$. Noting that both GAM and ZFZF can regulate DWs at different rates, nonlinear self-couplings of GAMs then have potential implications for the nonlinear dynamics of DWs and thus, fluctuation induced transport.

Finally, in section 6, a 'unified theoretical framework of GAM/EGAM' is constructed, consistently including of all the physics discussed through sections 2–4. It provides outlooks for important and challenging problems related to GAM, including (1) nonlinear dynamics of the coupled GAM-DW system, (2) nonlinear dynamics of EGAM and (3) nonlinear interactions of EGAM and DW. These problems are at the cutting edge of fusion research and will be topics of interest for the next decade.

Acknowledgments

This work is dedicated to late academician Changxuan Yu. This work is supported by National Natural Science Foundation of China under grant Nos. 11575157 and 11235009, the National Magnetic Confinement Fusion Research Program under Grants Nos. 2013GB104004 and 2013GB111004, Fundamental Research Fund for Chinese Central Universities under Grant No. 2017FZA3004, EUROfusion Consortium under grant agreement No. 633053 and US DoE Grants.

References

[1] Hasegawa A, Maclennan C G and Kodama Y 1979 *Phys. Fluids* **22** 2122
[2] Rosenbluth M N and Hinton F L 1998 *Phys. Rev. Lett.* **80** 724
[3] Spong D, Carreras B and Hedrick C 1994 *Phys. Plasmas* **1** 1503
[4] Zonca F, Chen L, Briguglio S, Fogaccia G, Vlad G and Wang X 2015 *New J. Phys.* **17** 013052
[5] Diamond P H, Itoh S-I, Itoh K and Hahm T S 2005 *Plasma Phys. Control. Fusion* **47** R35
[6] Horton W 1999 *Rev. Mod. Phys.* **71** 735
[7] Dimits A M *et al* 2000 *Phys. Plasmas* **7** 969
[8] Chen L and Zonca F 2007 *Nucl. Fusion* **47** 886
[9] Wagner F *et al* 1982 *Phys. Rev. Lett.* **49** 1408
[10] Wagner F 2007 *Plasma Phys. Control. Fusion* **49** B1
[11] Winsor N, Johnson J L and Dawson J M 1968 *Phys. Fluids* **11** 2448
[12] Zonca F and Chen L 2008 *Europhys. Lett.* **83** 35001
[13] Jakubowski M, Fonck R J and McKee G R 2002 *Phys. Rev. Lett.* **89** 265003
[14] Fujisawa A *et al* 2004 *Phys. Rev. Lett.* **93** 165002
[15] Melnikov A V *et al* 2006 *Plasma Phys. Control. Fusion* **48** S87
[16] Ido T *et al* 2006 *Nucl. Fusion* **46** 512
[17] Conway G D, Scott B, Schirmer J, Reich M, Kendl A and The ASDEX Upgrade Team 2005 *Plasma Phys. Control. Fusion* **47** 1165
[18] Liu A D *et al* 2009 *Phys. Rev. Lett.* **103** 095002
[19] Liu A D, Lan T, Yu C X, Zhang W, Zhao H L, Kong D F, Chang J F and Wan B N 2010 *Plasma Phys. Control. Fusion* **52** 085004
[20] Zhao K J *et al* 2006 *Phys. Rev. Lett.* **96** 255004
[21] Kong D *et al* 2013 *Nucl. Fusion* **53** 113008
[22] Kong D *et al* 2013 *Nucl. Fusion* **53** 123006
[23] Xu G S, Wan B N, Song M and Li J 2003 *Phys. Rev. Lett.* **91** 125001
[24] Nagashima Y *et al* 2005 *Phys. Rev. Lett.* **95** 095002
[25] Lan T *et al* 2008 *Plasma Phys. Control. Fusion* **50** 045002
[26] Chen L, Lin Z and White R 2000 *Phys. Plasmas* **7** 3129
[27] Xu Y H, Yu C X, Luo J R, Mao J S, Liu B H, Li J G, Wan B N and Wan Y X 2000 *Phys. Rev. Lett.* **84** 3867
[28] Berk H, Boswell C, Borba D, Figueiredo A, Johnson T, Nave M, Pinches S, Sharapov S and J. E. contributors 2006 *Nucl. Fusion* **46** S888
[29] Nazikian R *et al* 2008 *Phys. Rev. Lett.* **101** 185001
[30] Chen L 1994 *Phys. Plasmas* **1** 1519
[31] Zarzoso D *et al* 2013 *Phys. Rev. Lett.* **110** 125002
[32] Dumont R J *et al* 2013 *Plasma Phys. Control. Fusion* **55** 124012
[33] Nazikian R 2009 private communication

[34] Zhang H, Qiu Z, Chen L and Lin Z 2009 *Nucl. Fusion* **49** 125009
[35] FU G Y 2011 *J. Plasma Phys.* **77** 457
[36] Qiu Z, Chavdarovski I, Biancalani A and Cao J 2017 *Phys. Plasmas* **24** 072509
[37] Chen L, Qiu Z and Zonca F 2014 *Europhys. Lett.* **107** 15003
[38] Qiu Z, Zonca F and Chen L 2011 *Plasma Sci. Technol.* **13** 257
[39] Qiu Z, Chen L and Zonca F 2009 *Plasma Phys. Control. Fusion* **51** 012001
[40] Palermo F, Biancalani A, Angioni C, Zonca F and Bottino A 2016 *Europhys. Lett.* **115** 15001
[41] Biancalani A, Palermo F, Angioni C, Bottino A and Zonca F 2016 *Phys. Plasmas* **23** 112115
[42] Zonca F, Chen L and Qiu Z 2008 Kinetic theory of geodesic acoustic modes: radial structures and nonlinear excitations *Proc. 22nd IAEA FEC (Vienna, Italy)* CD-ROM file TH/P3-7
[43] Qiu Z, Zonca F and Chen L 2010 *Plasma Phys. Control. Fusion* **52** 095003
[44] Qiu Z, Zonca F and Chen L 2012 *Phys. Plasmas* **19** 082507
[45] Chen L, Qiu Z and Zonca F 2018 *Phys. Plasmas* **25** 014505
[46] Qiu Z, Chen L and Zonca F 2014 *Phys. Plasmas* **21** 022304
[47] Zhao H *et al* 2010 *Plasma Sci. Technol.* **12** 262
[48] Chen L and Hasegawa A 1974 *Phys. Fluids* **17** 1399
[49] Hasegawa A and Chen L 1976 *Phys. Fluids* **19** 1924
[50] Itoh S-I, Itoh K, Sasaki M, Fujisawa A, Ido T and Nagashima Y 2007 *Plasma Phys. Control. Fusion* **49** L7
[51] Chen L, Zonca F and Qiu Z 2010 Theoretical studies of GAM dynamics *Presented at the joint Varenna-Lausanne International Workshop on Theory of Fusion Plasmas (Varenna, Italy)* 30 August–3 September
[52] Frieman E A and Chen L 1982 *Phys. Fluids* **25** 502
[53] Brizard A J 1995 *Phys. Plasmas* **2** 459
[54] Hahm T S 1988 *Phys. Fluids* **31** 2670
[55] Gao Z, Itoh K, Sanuki H and Dong J Q 2006 *Phys. Plasmas* **13** 100702
[56] Hinton F and Rosenbluth M 1999 *Plasma Phys. Control. Fusion* **41** A653
[57] Sugama H and Watanabe T-H 2006 *J. Plasma Phys.* **72** 825
[58] Xu X, Xiong Z, Gao Z, Nevins W and McKee G 2008 *Phys. Rev. Lett.* **100** 215001
[59] Xu X *et al* 2009 *Nucl. Fusion* **49** 065023
[60] Zhang W, Lin Z and Chen L 2008 *Phys. Rev. Lett.* **101** 095001
[61] Feng Z, Qiu Z and Sheng Z 2013 *Phys. Plasmas* **20** 122309
[62] Gao Z, Wang P and Sanuki H 2008 *Phys. Plasmas* **15** 074502
[63] Gao Z 2010 *Phys. Plasmas* **17** 092503
[64] Biancalani A *et al* 2017 *Phys. Plasmas* **24** 062512
[65] Wang L, Dong J Q, Shen Y and He H D 2011 *Plasma Phys. Control. Fusion* **53** 095014
[66] Zhang H S and Lin Z 2010 *Phys. Plasmas* **17** 072502
[67] Wang L, Dong J Q, Shen Y and He H D 2011 *Phys. Plasmas* **18** 052506
[68] Zhou D 2007 *Phys. Plasmas* **14** 104502
[69] Smolyakov A, Nguyen C and Garbet X 2008 *Plasma Phys. Control. Fusion* **50** 115008
[70] Zhou D 2016 *Phys. Plasmas* **23** 102503
[71] Angelino P *et al* 2008 *Phys. Plasmas* **15** 062306
[72] Ido T *et al* 2015 *Nucl. Fusion* **55** 083024
[73] Horváth L *et al* 2016 *Nucl. Fusion* **56** 112003
[74] Qiu Z, Zonca F and Chen L 2014 *Excitation of Kinetic Geodesic Acoustic Modes by Drift Waves in Nonuniform Plasmas (Berlin, Germany)* ECA vol 38F (EPS) Paper No. P4.004.
[75] Zarzoso D, Migliano P, Grandgirard V, Latu G and Passeron C 2017 *Nucl. Fusion* **57** 072011
[76] Fu G 2008 *Phys. Rev. Lett.* **101** 185002
[77] Berk H and Zhou T 2010 *Nucl. Fusion* **50** 035007
[78] Zarzoso D, Garbet X, Sarazin Y, Dumont R and Grandgirard V 2012 *Phys. Plasmas* **19** 022102
[79] Wang H, Todo Y and Kim C C 2013 *Phys. Rev. Lett.* **110** 155006
[80] Girardo J-B, Zarzoso D, Dumont R, Garbet X, Sarazin Y and Sharapov S 2014 *Phys. Plasmas* **21** 092507
[81] Zarzoso D, Biancalani A, Bottino A, Lauber P, Poli E, Girardo J-B, Garbet X and Dumont R 2014 *Nucl. Fusion* **54** 103006
[82] Wang H, Todo Y, Ido T and Osakabe M 2015 *Phys. Plasmas* **22** 092507
[83] Sasaki M, Kasuya N, Itoh K, Hallatschek K, Lesur M, Kosuga Y and Itoh S-I 2016 *Phys. Plasmas* **23** 102501
[84] Cao J, Qiu Z and Zonca F 2016 *Phys. Plasmas* **22** 124505
[85] Sasaki M, Itoh K and Itoh S-I 2011 *Plasma Phys. Control. Fusion* **53** 085017
[86] Zonca F, Chen L, Briguglio S, Fogaccia G, Milovanov A V, Qiu Z, Vlad G and Wang X 2015 *Plasma Phys. Control. Fusion* **57** 014024
[87] Zonca F and Chen L 2000 *Phys. Plasmas* **7** 4600
[88] Chavdarovski I, Schneller M, Qiu Z, Biancalani A and Cao J 2017 Excitation of egams by the velocity anisotropy of ion beam with slowing down and maxwellian distribution *Nucl. Fusion* to be submitted
[89] Stix T H 1972 *Plasma Phys.* **14** 367
[90] Biancalani A, Chavdarovski I, Qiu Z, Bottino A, Del Sarto D, Ghizzo A, Gurcan O, Morel P and Novikau I 2017 *J. Plasma Phys.* **83** 725830602
[91] Li J *et al* 2013 *Nat. Phys.* **9** 817
[92] Biancalani A, Bottino A, Lauber P and Zarzoso D 2014 *Nucl. Fusion* **54** 104004
[93] Wang L, Dong J Q, He Z, He H and Shen Y 2014 *Phys. Plasmas* **21** 072511
[94] Biancalani A, Chavdarovski I, Qiu Z, Bottino A, Del Sarto D, Ghizzo A, Gurcan O, Morel P and Novikau I 2017 Nonlinear gyrokinetic investigation of energetic-particle-driven geodesic acoustic modes *Presented at the 17th European Fusion Theory Conf. (Athens, Greece)*
[95] Ren H 2017 *Nucl. Fusion* **57** 016023
[96] Vlad G, Zonca F and Briguglio S 1999 *Riv. Nuovo Cimento* **22** 1
[97] Chen L, White R B and Rosenbluth M N 1984 *Phys. Rev. Lett.* **52** 1122
[98] Chen L and Zonca F 2016 *Rev. Mod. Phys.* **88** 015008
[99] Zonca F and Chen L 2014 *Phys. Plasmas* **21** 072121
[100] Kaku M 1993 *Quantum Field Theory: A Modern Introduction* (New York: Oxford University Press)
[101] O'Neil T 1965 *Phys. Fluids* **8** 2255
[102] Berk H, Breizman B and Petviashvili N 1997 *Phys. Lett.* A **234** 213
[103] O'Neil T M and Malmberg J H 1968 *Phys. Fluids* **11** 1754
[104] O'Neil T M, Winfrey J H and Malmberg J H 1971 *Phys. Fluids* **14** 1204
[105] White R B, Goldston R J, McGuire K, Boozer A H, Monticello D A and Park W 1983 *Phys. Fluids* **26** 2958
[106] Vlad G, Briguglio S, Fogaccia G, Zonca F, Fusco V and Wang X 2013 *Nucl. Fusion* **53** 083008
[107] Wang X, Briguglio S, Chen L, Di Troia C, Fogaccia G, Vlad G and Zonca F 2012 *Phys. Rev.* E **86** 045401
[108] Zhang H S, Lin Z and Holod I 2012 *Phys. Rev. Lett.* **109** 025001
[109] Hahm T S, Beer M A, Lin Z, Hammett G W, Lee W W and Tang W M 1999 *Phys. Plasmas* **6** 922
[110] Lin Z, Hahm T S, Lee W W, Tang W M and White R B 1998 *Science* **281** 1835
[111] Sagdeev R and Galeev A 1969 *Nonlinear Plasma Theory* (AW Benjamin Inc.)
[112] Kaw P K and Dawson J M 1969 *Phys. Fluids* **12** 2586

[113] Chakrabarti N, Guzdar P N, Kleva R G, Naulin V, Rasmussen J J and Kaw P K 2008 *Phys. Plasmas* **15** 112310
[114] Guzdar P N, Chakrabarti N, Singh R and Kaw P K 2008 *Plasma Phys. Control. Fusion* **50** 025006
[115] Guzdar P N, Kleva R G, Chakrabarti N, Naulin V, Rasmussen J J, Kaw P K and Singh R 2009 *Phys. Plasmas* **16** 052514
[116] Chakrabarti N, Singh R, Kaw P K and Guzdar P N 2007 *Phys. Plasmas* **14** 052308
[117] Yu J, Dong J, Li X X, Du D and Gong X Y 2012 *J. Plasma Phys.* **78** 651
[118] Yu J and Dong J 2010 *Phys. Scr.* **82** 045504
[119] Qiu Z, Chen L and Zonca F 2014 *Nucl. Fusion* **54** 033010
[120] Hager R and Hallatschek K 2012 *Phys. Plasmas* **19** 082315
[121] Hager R and Hallatschek K 2012 *Phys. Rev. Lett.* **108** 035004
[122] Lang J, Chen Y and Parker S E 2007 *Phys. Plasmas* **14** 082315
[123] Lang J, Parker S E and Chen Y 2008 *Phys. Plasmas* **15** 055907
[124] Dannert T and Jenko F 2005 *Phys. Plasmas* **12** 072309
[125] Waltz R E and Holland C 2008 *Phys. Plasmas* **15** 122503
[126] Liu F, Lin Z, Dong J Q and Zhao K J 2010 *Phys. Plasmas* **17** 112318
[127] Liao X, Lin Z, Holod I, Li B and Sun G Y 2016 *Phys. Plasmas* **23** 122305
[128] Lan T *et al* 2008 *Phys. Plasmas* **15** 056105
[129] Zhong W *et al* 2015 *Nucl. Fusion* **55** 113005
[130] Melnikov A, Eliseev L, Lysenko S, Ufimtsev M and Zenin V 2017 *Nucl. Fusion* **57** 115001
[131] Rosenbluth M N 1972 *Phys. Rev. Lett.* **29** 565
[132] Zonca F, White R B and Chen L 2004 *Phys. Plasmas* **11** 2488
[133] Hasegawa A and Mima K 1978 *Phys. Fluids* **21** 87
[134] Guo Z, Chen L and Zonca F 2009 *Phys. Rev. Lett.* **103** 055002
[135] Singh R, Singh R, Kaw P, Gürcan O D and Diamond P H 2014 *Phys. Plasmas* **21** 102306
[136] Guzdar P N, Kleva R G and Chen L 2001 *Phys. Plasmas* **8** 459
[137] Chen L, White R B and Zonca F 2004 *Phys. Rev. Lett.* **92** 075004
[138] Qiu Z, Chen L and Zonca F 2013 *Europhys. Lett.* **101** 35001
[139] Adam J C, Tang W M and Rutherford P H 1976 *Phys. Fluids* **19** 561
[140] Tang W 1978 *Nucl. Fusion* **18** 1089
[141] Catto P J and Tsang K T 1978 *Phys. Fluids* **21** 1381
[142] Cheng C and Chen L 1981 *Nucl. Fusion* **21** 403
[143] Ernst D R, Lang J, Nevins W M, Hoffman M, Chen Y, Dorland W and Parker S 2009 *Phys. Plasmas* **16** 055906
[144] Xiao Y and Lin Z 2009 *Phys. Rev. Lett.* **103** 085004
[145] Zonca F, Lin Y and Chen L 2015 *Europhys. Lett.* **112** 65001
[146] Chen L and Zonca F 2011 *Europhys. Lett.* **96** 35001
[147] Zonca F and Chen L 1996 *Phys. Plasmas* **3** 323
[148] Mett R R and Mahajan S M 1992 *Phys. Fluids* B **4** 2885
[149] Qiu Z, Chen L and Zonca F 2017 Nonlinear decay and plasma heating by toroidal alfvén eigenmode *Phys. Rev. Lett.* submitted to
[150] Cheng C, Chen L and Chance M 1985 *Ann. Phys.* **161** 21
[151] Fu G Y and Van Dam J W 1989 *Phys. Fluids* B **1** 1949
[152] Chen L 1988 *Theory of Fusion Plasmas* ed J Vaclavik *et al* (Bologna: Association EUROATOM) p 327
[153] Chen L and Zonca F 2012 *Phys. Rev. Lett.* **109** 145002
[154] Qiu Z, Chen L and Zonca F 2016 *Phys. Plasmas* **23** 090702
[155] Qiu Z, Chen L and Zonca F 2016 *Nucl. Fusion* **56** 106013
[156] Qiu Z, Chen L and Zonca F 2017 *Nucl. Fusion* **57** 056017
[157] Chen L and Zonca F 2013 *Phys. Plasmas* **20** 055402
[158] Chen L and Hasegawa A 1991 *J. Geophys. Res.: Space Phys.* **96** 1503
[159] Chen L, Lin Z, White R B and Zonca F 2001 *Nucl. Fusion* **41** 747
[160] Zonca F and Chen L 1993 *Phys. Fluids* B **5** 3668
[161] Hahm T S and Chen L 1995 *Phys. Rev. Lett.* **74** 266
[162] Zonca F, Romanelli F, Vlad G and Kar C 1995 *Phys. Rev. Lett.* **74** 698
[163] Chen L, Zonca F, Santoro R and Hu G 1998 *Plasma Phys. Control. Fusion* **40** 1823
[164] Ido T *et al* 2006 *Plasma Phys. Control. Fusion* **48** S41
[165] Xu Y *et al* 2011 *Plasma Phys. Control. Fusion* **53** 095015
[166] Hamada Y, Watari T, Nishizawa A, Yamagishi O, Narihara K, Kawasumi Y, Ido T, Kojima M, Toi K and The JIPPT-IIU Group 2012 *Nucl. Fusion* **52** 063023
[167] Li Z, Dong J, Sheng Z, Yu M Y and Wang W 2017 *Phys. Plasmas* **24** 102507
[168] Kong D *et al* 2017 *Nucl. Fusion* **57** 044003
[169] Qiu Z, Chen L and Zonca F 2015 *Phys. Plasmas* **22** 042512
[170] White R, Kaw P, Pesme D, Rosenbluth M, Laval G, Huff R and Varma R 1974 *Nucl. Fusion* **14** 45
[171] Zhao K J *et al* 2010 *Plasma Phys. Control. Fusion* **52** 124008
[172] Conway G D, Troster C, Scott B, Hallatschek K and The ASDEX Upgrade Team 2008 *Plasma Phys. Control. Fusion* **50** 055009
[173] Nagashima Y *et al* 2007 *Plasma Phys. Control. Fusion* **49** 1611
[174] Brizard A J and Hahm T S 2007 *Rev. Mod. Phys.* **79** 421
[175] Sasaki M, Itoh K, Nagashima Y, Ejiri A and Takase Y 2009 *Phys. Plasmas* **16** 022306
[176] Sasaki M, Itoh K, Ejiri A and Takase Y 2009 *Plasma Phys. Control. Fusion* **51** 085002